Multi-omic Analysis of Hibernator Skeletal Muscle and Regulation of Calcium Handling

A Thesis
SUBMITTED TO THE FACULTY OF
UNIVERSITY OF MINNESOTA
BY

Kyle J. Anderson

IN PARTIAL FULFILLMENT OF THE REQUIREMENTS
FOR THE DEGREE OF
MASTER OF SCIENCE

Advisor: Matthew T. Andrews

May 2016

Acknowledgements

I would like to first thank my family and friends for their guidance and support through my graduate career. I would also like to thank my thesis committee Dr. Andrews, Dr. Hampton, and Dr. Liang for their guidance and assistance throughout these projects. None of this work would have been possible without the financial support I received from the Biology department through my GTA appointments. Additional financial and scientific support to complete the proteomics project came from Tim Griffin and everyone at the Center for Mass Spectrometry and Proteomics at the University of Minnesota and was greatly appreciated.

This work was funded by the United States Army Medical Research and Materiel Command contract W81XWH-11-0409, the University of Minnesota McKnight Presidential Endowment, and NIH grant 1RC2HL101625-01 to M.T.A. Additional funding came from the NSF grant 1147079 for the Galaxy-P team.

Abstract

Mammalian hibernation is a strategy employed by many species to survive fluctuations in resource availability and environmental conditions. Hibernating mammals endure conditions of dramatically depressed heart rate, body temperature, and oxygen consumption; yet do not show the typical pathological responses. Because of the high abundance and metabolic cost of skeletal muscle, not only must it adjust to the constraints of hibernation, but it is also positioned to play a more active role in the initiation and maintenance of the hibernation phenotype. My M.S. thesis research has primarily focused on the generation and analysis of two high-throughput 'omics screens in thirteen-lined ground squirrel skeletal muscle. A transcriptomic analysis using Illumina HiSeq2000 technology identified 1,466 differentially expressed genes throughout their circannual cycle. This RNAseq data allowed for greater protein identifications in an iTRAQ based proteogeomic analysis of the same animals. Of the 1,563 proteins identified by this proteogenomic approach, 232 were differentially expressed. These data support previously reported physiological transitions, while also offering new insight into specific mechanisms of how hibernator muscles might be reducing nitrogenous waste, preserving mass and function, and signaling to other tissues. Sarcolipin is a specific gene of interest that shows a 10-fold difference in expression between hibernation and spring collection points. Because of sarcolipin's interaction with the SERCA pump and their role in muscle-based thermogenesis and calcium homeostasis bioenergetics, I have developed methods to measure the consequences of this differential expression.

Table of Contents

List of Tables……iv

List of Figures……...v

Introduction……..……1

Chapter 1. Transcriptome Analysis

Materials and Methods……9

Results……15

Discussion……...21

Chapter 2. Proteomic Analysis

Materials and Methods…….29

Results and Discussion……34

Chapter 3. Future Directions--Calcium Handling Efficiency

Materials and Methods…….48

Results and Discussion……55

Future Directions……...59

References…….62

List of Tables

		Page
Table 1	Overview of Illumina HiSeq2000 RNAseq Data	15
Table 2	Pairwise Differential Expression	17

List of Figures

		Page
Figure 1	Circannual cycle of a thirteen-lined ground squirrel and sample collection points	2
Figure 2	Most Abundant Transcripts	16
Figure 3	Gene expression changes supporting an increased reliance on fatty acid metabolism during hibernation	18
Figure 4	Gene expression changes supporting an increase in oxidative capacity preceding and during hibernation	20
Figure 5	Gene expression changes supporting a shift in protein turnover during hibernation	21
Figure 6	Sampling design, preparation, and iTRAQ labeling	33
Figure 7	Major categorizations made by DAVID analysis of all differentially expressed proteins	35
Figure 8	Abundance profile of metabolism-related proteins	37
Figure 9	Abundance profile of contractile/structural proteins	39
Figure 10	Relative protein abundance of AMPD1 and FMOD for 6 comparisons made throughout the circannual cycle	41
Figure 11	Abundance profile of mitochondrial proteins	42
Figure 12	Differentially expressed transcripts and their protein products	47
Figure 13	SERCA coupling ratio in hibernation and spring	57
Figure 14	Expression profiles of calcium handling proteins in hibernator skeletal muscle	58
Figure 15	Sarcolipin gene expression	59

Introduction

Mammalian Hibernation

Hibernation is a strategy employed by a number of mammalian species to survive seasonal periods of low resource availability. These seasonal fluctuations can be wet and dry seasons in the tropics, or cold and warm seasons at higher latitudes. In either case, the goal of hibernation is the same: to reduce metabolic activity and preserve energy and other limiting resources. This survival strategy is seen in species throughout the class Mammalia (1), suggesting that the ability to hibernate is a conserved trait amongst all mammals, rather than a specific adaptation that has evolved independently many times. Thus, it is the differential expression of genes present in all mammals that allows for the hibernation phenotype, not a specific set of hibernation genes.

The work in this thesis uses the thirteen-lined ground squirrel (*Ictidomys tridecemlineatus*) as a model of hibernation. These animals are "deep hibernators," meaning that hibernation consists of long bouts of torpor (TOR) interrupted by brief inter bout arousals (IBA) (Figure 1). When a thirteen-lined ground squirrel enters torpor, they reduce their core body temperature (T_b) to near ambient (5-10°C), they reduce their heart rate to 3-10 bpm from 300-400 bpm when active, and their oxygen consumption can be as low as 2% of normal, active levels. They remain in this motionless state for 7-10 days before rewarming themselves for an IBA (2,3). The rewarming process is initially mediated by the activity of brown adipose tissue, which uses uncoupling protein 1 to generate heat from the mitochondrial proton gradient (4). After their muscles reach a temperature of around 16°C they begin shivering to contribute to rewarming (5). These animals will warm their bodies from 5 to 37°C over the course of a couple of

hours (2). During an IBA, they maintain a body temperature around 37°C, their heart rate is 300-400 bpm, and their oxygen consumption is that of a normal active animal (2). After remaining in this euthermic state for 12-24 hours, they again allow their bodies to passively cool for another bout of torpor. They repeat this torpor-arousal cycle numerous times throughout the hibernation season (Figure 1). During the 5-6 months that these animals hibernate, they do not consume any food. Instead, they rely on fat deposits that they have accumulated during the spring, summer and fall (3). Even when these animals are allowed food ad libitum, they go through a hyper to hypo-phagic transition in the fall during which they cease food consumption in preparation for hibernation (6).

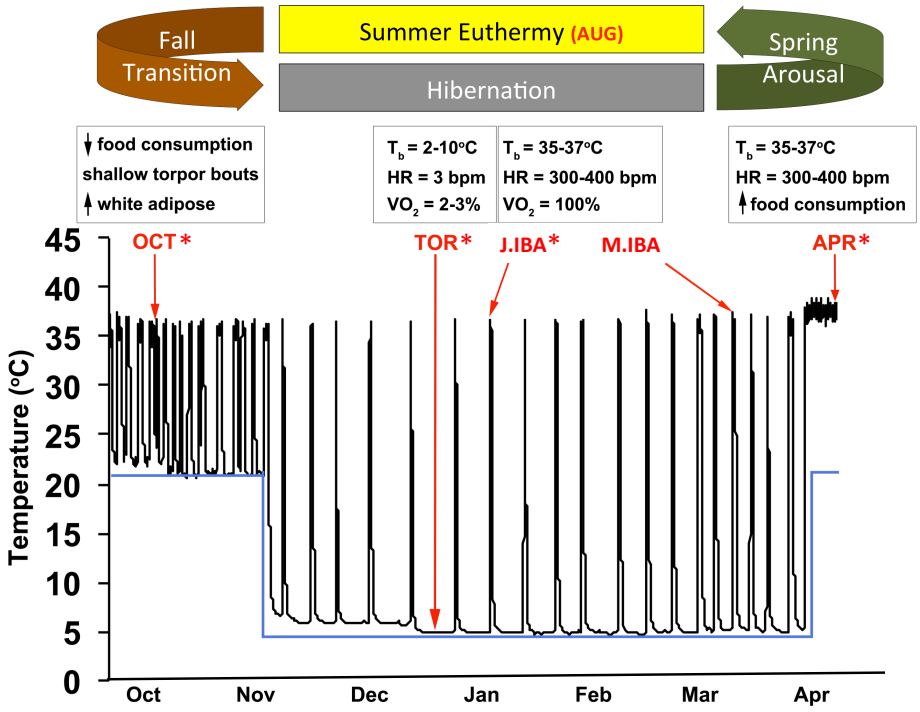

Figure 1. Circannual cycle of a thirteen-lined ground squirrel and sample collection points. The black line represents the core body temperature (T_b) of a single animal measured by a surgically implanted transmitter. The blue line represents ambient temperature (T_a). Red text indicates representative times and T_b at which animals were collected. All indicated collection points were used to generate proteomic data, while collection points with asterisks were used to generate transcriptomic data.

Because these regular IBAs are very energetically expensive, they are thought to serve some vital functions that allow these animals to survive the harsh conditions of hibernation (7). It is well documented that transcription and translation do not occur at the low T_b of torpor (8,9). It is likely however that protein degradation still occurs at these low temperatures, though at a slower rate. The most likely function of the IBAs is to allow these animals to replenish mRNAs and proteins that may degrade during TOR, but are essential for survival and continuing the hibernating phenotype.

Skeletal Muscle

Given the high abundance and metabolic cost of skeletal muscle, it seems reasonable that this tissue would not only have major challenges overcoming the physiological transitions associated with hibernation but would also contribute significantly to making these transitions possible on a whole-organism level. Skeletal muscle is the single most abundant tissue in the mammalian body, making up ~40% of total body mass and being responsible for 20-30% of resting metabolic demand (10). Additionally, the high plasticity of skeletal muscle in response to metabolic and functional demands make it an ideal target for hibernators to adjust whole-body physiological parameters with the alteration of a single tissue (11).

The physiological metrics of a given muscle fiber can lie within a wide spectrum, allowing different muscles to perform specific functions more efficiently and permitting a high degree of adaptability to new functions. There are typically four classifications to which a single muscle fiber can be assigned (11). These classifications are based on myosin isoform expression, but tightly correlate with contractile and metabolic properties such that fibers with a fast activation frequency and high force generation tend to have a more glycolytic metabolism, whereas fibers with a slower activation frequency and lower

force generation will have a more oxidative metabolism (12). Type IIB are the “fastest” fiber type. They express primarily myosin heavy chain 2B and rely heavily on a glycolytic metabolism (12). Because these fibers have relatively low mitochondrial densities and store a large amount of glycogen, these fibers are the largest and will appear white in color. Because of their reliance on glycogen, and their high-energy demands, fast muscles are quickly fatigable, but produce greater force than the other fiber types (12). Type I muscle fibers are the “slowest” fiber type. They primarily express myosin heavy chain β (interestingly, one of the two myosins expressed in the heart) and rely on oxidative metabolism (12). These are the smallest muscle fibers and appear red due to their high mitochondrial density (11). These muscles produce less force than the other fiber types, but can be activated for very long periods without fatigue. Type IIA and IIX are intermediate classifications that are known as fast oxidative muscles. These intermediate fiber types express myosin isoforms by the same name and on the scale from slow to fast, type IIA are “slower” than type IIX (11).

Skeletal muscle is highly plastic, meaning that it can readily transition between these different fiber types depending on functional or metabolic demands. It is widely accepted that the transitions must occur in a step-wise fashion from one fiber type to the next closest as in the scheme: I <> IIA <> IIX <> IIB (13). Not only can muscles change their composition to accommodate demands, but they can also grow or shrink. Muscle growth is referred to as hypertrophy and occurs during development, and in response to mechanical overload or anabolic hormonal stimulation such as testosterone or β_2-adronergic agonists (14). A reduction in muscle mass, or atrophy, results from aging, cancer, starvation, diabetes, disuse, loss of neuronal input, or catabolic hormone stimulation (corticosteroids) (14). Chronic disuse can cause a typical mammalian muscle to atrophy up to 30% over a two week period. Associated with this disuse

atrophy is a shift to a faster, more glycolytic fiber type (14,15). Muscle mass is maintained by a balance between the continuous processes of protein synthesis and degradation. A shift in this balance will result in muscle hypertrophy or atrophy (14).

Finally, in an animal that regularly changes its core body temperature by as much as 35°C, thermoregulation and its energetics are important aspects of skeletal muscle function. At rest, skeletal muscle is responsible for 20-30% of whole body metabolism (10). Much of this energy is used to maintain ion gradients necessary for excitation contraction coupling (16). Particularly, the calcium concentration within the sarcoplasmic reticulum (SR) can be as high as four orders of magnitude greater than that of the cytoplasm (17). The release of this calcium store by ryanodine receptors is necessary to allow actin-myosin crosslinking and subsequent muscle contraction. This calcium is then pumped back into the SR by the action of sarco-endoplasmic reticulum calcium ATPase (SERCA). This pump hydrolyzes ATP to pump calcium back into the SR. The action of this pump, even at resting conditions, accounts for 40-50% of muscle metabolism (16). During muscle activity, much of the ATP being utilized by a muscle cell is to pump calcium or initiate actin-myosin binding, but some of the energy is inevitably released as heat (18). This is what makes shivering is an effective method of thermogenesis. Sarcolipin is a small protein than interacts with SERCA in such a way to uncouple ATP hydrolysis from calcium pumping (19). This means that more ATP must be hydrolyzed to pump the same amount of calcium. This results in more heat generation in muscle and a greater energy demand for maintaining calcium homeostasis. This mechanism has recently been shown to play a major role in mammalian thermogenesis, such that mice lacking sarcolipin cannot maintain normal body temperature when cold-challenged (20).

Hibernator Skeletal Muscle

For the 5-6 months of hibernation, the thirteen-lined ground squirrel is almost completely immobile, shivering briefly during an arousal and moving very little during an IBA. Despite this level of disuse their muscles maintain greater tone and functionality than would be expected in a non-hibernating mammal under similar conditions (21). Additionally, these animals display a fast to slow muscle fiber type transition in the months leading up to hibernation. In the plantaris and gastrocnemius muscles of golden mantle ground squirrels (*Spermophilus lateralis*) Nowell et al. demonstrated a significant reduction in myosin 2B and an increase in myosin 2X between September and October, demonstrating this fast to slow transition (22). This fiber-type shift was maintained and even continued slightly through the hibernation season, likely through the activation of the exercise endurance pathway and the activity of the transcriptional coactivator PGC-1α (23). By transitioning to a slower, more oxidative fiber type prior to hibernation, their muscles are more adapted to utilize the lipid-based metabolism required during hibernation.

Maintaining contractile function despite extended disuse is another important demand placed on hibernator skeletal muscle. The initial stages of rewarming are mediated by non-shivering thermogenesis in brown adipose tissue (BAT), while the later stages also make use of shivering thermogenesis in skeletal muscle (5). In the spring, these hibernators arouse to an environment full of predatory mammals and birds that are hungry after a long winter or migration. Functional muscles are essential to forage, evade predation, and successfully reproduce. In addition to the potential effects of PGC-1α expression, a variety of mechanisms have been proposed to maintain hibernator muscle. Andres-Mateos et al. demonstrated the role of serum/glucocorticoid-induced kinase in maintaining protein synthesis/degradation balance in hibernation (21).

Various research groups including ours have demonstrated a decrease in mRNA and protein abundance of myostatin, a negative regulator of muscle mass, during the bulk of hibernation (24, 25). Another hypothesis, one also supported by our proteome data, is that these animals undergo a period of muscle regrowth during the final stages of hibernation, in preparation for the final spring arousal (26).

The need for these animals to maintain adequate muscle mass and function is at odds with their need to conserve energy during hibernation. With up to 15% of total body metabolism attributed to the action of the SERCA pump in skeletal muscles, this pump is an ideal target for energy conservation (10,17). The role of the sarcolipin protein is to reduce the efficiency of SERCA such that it hydrolyzes more ATP and produces more heat (19). Mechanisms of muscle-based thermogenesis such as this have only recently gained new interest in model organisms (20), but our hibernator may represent a more useful model since their thermoregulatory needs vary throughout the year.

Focus of Thesis

Because of its abundance and metabolic demand, slight changes in skeletal muscle physiology can have significant effects body-wide, likely making it an important contributing factor to the hibernation phenotype. For this reason, we have taken a multi-omic approach to describe changes in muscle physiology throughout the circannual cycle of these animals. These methods have yielded many hypotheses, both novel and supported by previous research.

Characterizing the physiological transitions these animals make throughout the year and understanding the regulation behind these transitions has broad biomedical applications. There is currently no treatment to prevent the loss of muscle mass

associated with a variety of pathologies. Understanding how these animals maintain muscle tone and function despite months of disuse could eventually lead to the development of such treatments. With the recent initiative to send humans to Mars, the idea of long-term space travel and the need for muscle preservation is becoming more fact than fiction. Metabolically, the endogenous control these animals seem to have over their muscle metabolism could lead to therapies with the potential to reduce the current obesity trend in developed nations.

To understand how hibernators are altering their muscle physiology, we used Illumina high-throughput sequencing technology to analyze mRNA levels in their skeletal muscles at four time-points throughout the year (27). The advancements in sequencing technology are such that this study was able to identify almost seven times as many genes as a similar study done with hibernator cardiac muscle in our lab 10 years ago and with much higher accuracy for quantification (28). Using this sequence data, we also performed an iTRAQ based MS/MS shotgun proteomics screen using the same animals as in the transcriptome with two additional time points (29). This proteogenomic approach led to greater protein identification and quantification than using genomic predictions alone and analyzing these two datasets together allowed for greater interrogation of regulatory processes between mRNA and protein expression. Various projects have arisen from this data, one of which being to examine SERCA efficiency throughout the year to determine its contribution to thermogenesis and muscle metabolism. From projects like this, it is our goal that these expression data will allow us to expand our knowledge of hibernator physiology and potentially inspire novel therapies for human use.

Chapter 1: Transcriptome Analysis

Materials and Methods

Animals

Thirteen-lined ground squirrels were live-trapped near Paynesville, MN and housed in the Association for Assessment and Accreditation of Laboratory Animal Care-accredited Animal Care Facility at the University of Minnesota Duluth School of Medicine. Squirrels were individually housed in plastic top-load rat cages with aspen shavings. The squirrels were housed under standard conditions in a 12:12 light/dark cycle at 23°C and fed standard rodent chow and water *ad libitum* from April to October. During the hibernation season (November-March) the squirrels were moved into an artificial hibernation chamber and kept in constant darkness at 5-7°C with no food provided and water *ad libitum*. All experimental animal procedures were approved by the University of Minnesota Institutional Animal Care and Use Committee (protocol #1103A97712).

Experimental Collection Points

Four collection points were chosen for these experiments to reveal the most meaningful comparisons in ground squirrel skeletal muscle across the hibernation season. The four collection points used were: pre-hibernation (OCT), torpor (TOR), during an interbout arousal (IBA), and post-hibernation (APR) (Figure 1). Three males and three females were sacrificed at each collection point. Animal state at each collection point was determined by rectal temperature and animal behavior. All animals were collected between 10 am and 3 pm.

For the OCT collection point the animals have increased body mass in the preceding months and are preparing for hibernation. October animals are experiencing torpor bouts, in which body temperature drops as low as 20°C for up to 24 hours. This time point represents an opportunity to detect transcriptional changes associated with preparation for hibernation. October active animals were collected in the first two weeks of October and were active at the time of sacrifice, with a body temperature of 35-37°C and were observed as awake and active (open eyes and coordinated body movements).

The TOR and IBA collection points reflect the extreme conditions that hibernating ground squirrels experience. These collection points are important in showing the changes that orchestrate the drastic physiological changes associated with the torpor-arousal cycle. The saw dusting method was used to identify squirrels in TOR and IBA. TOR animals were collected after a minimum of three days in a torpor bout, and showed no visible signs of arousal. At the time of sacrifice, rectal temperatures were taken to verify torpid state (T_b 6-8°C). Animals collected for the IBA collection point aroused naturally and were awake, active, and showed coordinated body movement. Rectal temperatures collected at sacrifice showed an active body temperature between 35-37°C. Torpor and IBA animals were collected in January and February, when torpor bouts are the longest.

The APR collection point reflects the post-hibernation state of the animal, when the animal is recovering from the hibernation season, resuming food consumption, and ready for reproduction. These animals were removed from the hibernation chambers at the end of March and returned to a 12:12 light/dark cycle at 23°C with food and water ad libitum. The animals for the APR collection point were collected in the second and third weeks of April.

Muscle Dissection

All animals were fully anesthetized with isofluorane and then sacrificed by decapitation. The quadriceps femoralis was removed from the upper thigh, further dissected into smaller pieces, and rapidly flash frozen in liquid nitrogen. The two quadriceps femoralis muscles are frozen and stored separately. The time from decapitation to sample freezing was less than 10 minutes. Tissues were stored at -80°C until RNA purification.

RNA Preparation

RNA was isolated using a Qiagen RNeasy Mini Kit and remaining genomic DNA was removed using an Ambion DNase kit. For RNA quality control, the protein concentration was determined using a Nanodrop and then one µg of each sample was run on an agarose gel looking for distinct 28s and 18s bands. RNA from one male and one female from each collection point were combined together in a single sample and each collection point contained three pooled samples. Samples were pooled to eliminate variation due to sex. Samples were sent to the University of Minnesota Biomedical Genomics Center (Minneapolis, MN) for Illumina HiSeq 2000 sequencing.

Sample Quality Assessment

Total RNA isolates were quantified using a fluorimetric RiboGreen assay. Total RNA integrity was assessed using capillary electrophoresis, and generated an RNA Integrity Number (RIN). All of the samples passed the initial Quality Control (QC) step verifying them as high quality samples (> 1 microgram, RIN=8+). RNA samples were converted to Illumina sequencing libraries using Illumina's Truseq RNA Sample Preparation Kit (RS-122-2001).

Library creation

From each replicate, one µg of total RNA (equal RNA from male and female) was enriched for mRNA using oligo-dT coated magnetic beads, fragmented and reverse transcribed into cDNA. The cDNA was fragmented, blunt-ended, and ligated to indexed (barcoded) adaptors and amplified using 15 cycles of PCR. Final library size distribution was validated using capillary electrophoresis and quantifed using PicoGreen fluorimetry and qPCR. Libraries were successfully sequenced for all samples.

Cluster generation and sequencing

Truseq libraries were hybridized to a paired-end flow cell and individual fragments were clonally amplified by bridge amplification on the Illumina cBot. Libraries were clustered at a concentration of 12pM. After clustering the flow cell was loaded on the HiSeq 2000 and sequenced using Illumina's Sequencing by Synthesis (SBS) chemistry. Upon completion of a read, a seven base pair index read was performed. Samples were run for 100 cycles with a minimum of 10 million single reads per sample. Base call (.bcl) files for each cycle of sequencing were generated by Illumina Real Time Analysis (RTA) software. The base call files and run folders were then exported to servers maintained at the Minnesota Supercomputing Institute (MSI, Minneapolis, MN). Primary analysis and de-multiplexing were performed using Illumina's CASAVA software 1.8.2, resulting in de-multiplexed FASTQ files.

Bioinformatics Analysis

Over 10 million raw sequence reads were generated per sample. These reads were mapped to a set of *I. tridecemlineatus* contigs assembled in the open-source

program Trinity (30). The contigs were constructed using consensus regions of DNA from this data in addition to previous *I. tridecemlineatus* RNAseq experimental data from brain cortex, hypothalamus (31), brown adipose tissue (BAT) (35), and white adipose tissue (WAT) (32). Trinity was used to predict coding domain subsequences within these contigs in order to specifically select for protein-coding transcripts. Any contig containing a predicted coding domain was selected and trimmed to include only this domain plus up to 100 bases on both ends of the domain. Before matching reads to the contigs, mitochondrially-encoded genes were screened out using the thirteen-lined ground squirrel mitochondrial genome sequence (32) and NCBI's megablast program (33) due to the high density of mitochondrial genomes in skeletal muscle. The selected contigs were then compared to the NCBI RefSeq human mRNA sequences using NCBI BLASTn (33). Raw reads from each experimental sample were identified using these contigs, and then quantified using the counts for each gene. Gene names used for identification are the official Human Genome Organisation (HUGO) Gene Nomenclature Committee (HGNC) designations.

Resulting read counts were normalized to the upper-quartile and then fitted to a negative binomial distribution using DESeq v1.6.1 (34). All genes included in the initial analysis had at least 10 read counts total across the four time points. All read counts across all collection points were quantified for each mRNA to determine overall abundance. Maximum fold change for each gene was calculated as the collection point with the highest average read counts by the collection point with the lowest average read counts. Tissue specificity was calculated for each gene by dividing the percentage of read counts in that tissue divided by the total number of read counts in all other transcriptomic samples, including heart, skeletal muscle, cortex, hypothalamus (31), BAT (35), and WAT (32), which were obtained from other transcriptomic experiments.

Differential gene expression

Differential gene expression was determined using an analysis of deviance in DESeq v1.6.1, to generate a test statistic (p-value) using the methods described by Anders and Huber (34). The computed p-values were independently filtered (36) by restricting those with at least a 50% change between any two collection points and at least one collection point with a mean of 100 or more reads. The Benjamini-Hochberg method was then used to correct for multiple comparisons, providing a p-value cutoff for significance, which controlled the false discovery rate (FDR) at 0.05. Any transcript with a p-value less than the respective cutoff value was considered differentially expressed (FDR<0.05). On these differentially expressed genes, post hoc pair-wise comparisons were performed using the same function in DESeq v1.6.1, but with different input data. For this pair-wise analysis, the p-values were independently filtered (36) to restrict to a 50% change between two specific collection points, rather than any two. The Benjamini-Hochberg method was used to control the FDR to 0.05 to correct for multiple comparisons.

Functional Annotation Clustering

The differentially expressed transcripts were analyzed using the functional annotation tools of DAVID (37) and literature searches. Genes were first sorted for differential expression relative to APR and then sorted for genes that were upregulated and downregulated. These lists were entered into DAVID separately for analysis. DAVID analysis provided annotation and gene GO-term enrichment analysis. DAVID functional annotation clustering (FAC) was used for further analysis (38). DAVID functional annotation clustering uses an algorithm to measure the relationships among

the annotation terms. Each annotation term inside each cluster is assigned a p-value (Fisher Exact/EASE score) and these p-values are used to calculate a Group Enrichment Score. This score is the geometric mean of the member's p-values in a corresponding annotation cluster and is used to rank their biological significance.

Results

The goal of this study was to use advanced high-throughput sequencing technology to determine changes in gene expression in hibernator skeletal muscle throughout the year. Total RNA was prepared at four time points throughout the circannual cycle: APR, OCT, TOR, and IBA (Figure 1). Illumina HiSeq2000 sequencing of cDNAs derived from 24 animals resulted in 109,274,656 reads of 100 bases (Table 1). Contig assembly resulted in the identification of 14,169 distinct transcripts. Only transcripts that had 10 reads at any time point were used for further analysis. This resulted in the identification of 8,278 protein-coding genes.

Table 1. ***Overview of Illumina HiSeq2000 RNAseq data***

High-quality reads	109,274,656
Distinct transcripts	14,169
Protein-coding genes	8,278
Differentially expressed genes	1,466

Ranked Abundance

As expected, many of the most abundant transcripts are for structural components of the sarcomere. Figure 2 shows the 20 most abundant transcripts, many of which are sarcomeric proteins. Few of these genes are differentially expressed, with *MYH2, MYH4*, and *ACTN2* differentially high in APR and *MB* differentially high in OCT.

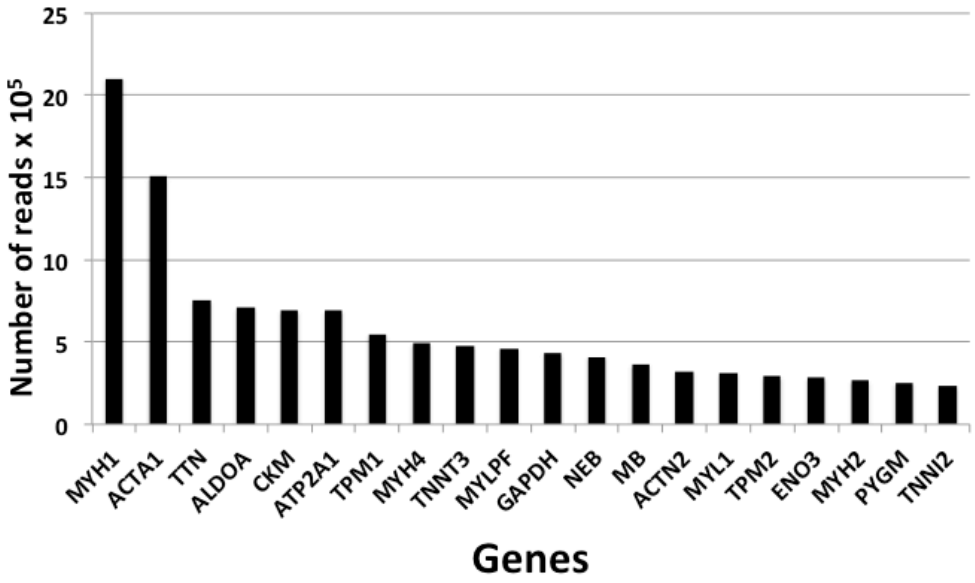

Figure 2. Most abundant transcripts. The total number of reads across all collection points for each mRNA were used to determine overall abundance. The 20 most abundant transcripts are represented.

Differential Expression

We determined differential expression across the four collection points by independently filtering p-values computed by DESeq. Genes are considered differentially expressed if they have at lease 100 normalized counts in one collection point and have at least a 50% fold change between the mean of any two points. Of the 8,278 transcripts identified, 1,466 were differentially expressed (Table 1). The five genes showing the greatest fold change were carbonic anhydrase 1 (*CA1*), Uroplakin 1A (*UPK1A*), Aldose Reductase-Related Protein (*AKR1B10*), Guanine Nucleotide-Binding Protein 6 (*GBP6*), and a Ctyochrome p450 family member (*CYP1A1*). With each of these genes, the highest expression was during the APR time point. The function of CA1 is to remove carbon dioxide from tissues by conversion to bicarbonate (39). UPK1A is an important protein in the bladder epithelium and is likely not expressed at the protein level in skeletal muscles. AKR1B10 is a member of the aldo-keto reductase

superfamily, capable of reducing various carbonyl substrates (40). GBP6 is a guanylate binding protein important for immunity against bacterial and viral infections (41). Finally, CYP1A1 is a monooxygenase involved in the metabolism of xenobiotics and is induced under hypoxic conditions (42,43). Post-hoc pairwise comparison between any two points showed that the highest number of statistically significant changes occurred between TOR and APR with 1,317 genes (Table 2). Interestingly, the comparison showing the fewest differences was between TOR and IBA with 109 genes.

Table 2. Pair-wise Differential expression

	APR	IBA	TOR
OCT	524	688	938
TOR	1,317	109	
IBA	1,085		

Functional Analysis

Fuel utilization

Differentially expressed genes were functionally clustered using the Database for Annotation, Visualization and Integrated Discovery (DAVID) to highlight functional pathways that are altered across the circannual cycle of a hibernator. Genes were first sorted by their expression relative to Apri, and then further sorted into genes that were upregulated or downregulated. There is evidence that mitochondrial function, including fatty acid metabolism, is especially important for the hibernation phenotype. Transcripts associated with fatty acid metabolism are upregulated in OCT, TOR, and IBA (Figure 3). We see increased expression of many of the key players utilized during fatty acid metabolism including *FABP3, ACOT1, ACSL1, ACSL4*, and *ACSL6.* These genes encode important enzymes in the conversion of free long-chain fatty acids into fatty-acyl

CoA. Fatty acids are transported across the mitochondrial membrane by CPT1A, CPT1B, and SLC25A20, all of which have significantly increased expression during hibernation. Additionally, gene expression of enzymes required for β-oxidation of fatty-acyl CoA is significantly upregulated, including *ACADS, ECH1, ACOT2, HADHA*, and *HADHB*. Catalase (CAT), and peroxiredoxin (PRDX5) are responsible for the breakdown of hydrogen peroxide produced in β-oxidation and both are upregulated beginning in OCT or throughout hibernation. Enzymes involved in the degradation of branched chain fatty acids are significantly downregulated, for example *ACADSB*. This is consistent with previous findings of reduced expression of proteins associated with mitochondrial β-oxidation of branched chain fatty acids (44).

Functional Category	*Gene Name*	Normalized mRNA Reads			
		April	October	Torpor	IBA
Converstion of long-chain fatty acids to fatty acyl-CoA	*FABP3*	6821	8509	11787*	12880
	ACOT1	325	416	717*	822
	ACSL1	2915	3927	5681*	4504
	ACSL3	84	82	128*	117
	ACSL4	316	398	634*	596
	ACSL6	77	106	114	140
Fatty-acyl CoA mitochondrial Transport	*CPT1A*	211	132	682*	593
	CPT1B	8978	12475	14111	12173
	SLC25A20	564	770	978*	990
B-oxidation of fatty-acyl CoA	*ACADS*	859	1444	1688*	1654
	ACADVL	7915	7856	9060	8964
	ACAD10	428	356	354	335
	ECH1	5116	6454	8081	7584
	ACOT2	99	121	213*	228
	HADHA	4584	7838	10228*	10867
	HADHB	6836	14497	18532*	19168
Branched-chain FA metabolism	*ACADSB*	781	385	244*	302
Lipotoxicity protection	*UCP3*	2105	755	2329*	1988
Breackdown H_2O_2	*CAT*	2256	1820	3049*	3043
	PRDX5	494	776	705	757

Figure 3. Gene expression changes supporting an increased reliance on fatty acid metabolism during hibernaiton. Genes are grouped into functional categories based on their role in fatty acid metabolism. Differential expression relative to April is signified by red (increased expression) or green (decreased expression) shading. Differential expression relative to October is signified by an asterisk.

Increased oxidative capacity

Supporting the increase in fatty acid metabolism genes, we also see a significant increase in a number of genes involved in oxygen transport and delivery to and within muscle cells. TCA cycle enzymes, including isocitrate dehydrogenase 3 (*IDH3A*) and aconitase (*ACO2*), increase beginning in OCT (Figure 4). TCA cycle products would then fuel the electron transfer system (ETS) and oxidative phosphorylation. Without seeing a clear increase in genes directly associated with the ETS and oxidative phosphorlyation, we see increases in genes involved in iron-protein assembly and oxygen transport. Angiogenic growth factors *VEGFA* and *VEGFB* show peak expression in OCT and elevated expression in hibernation, while *ADAMTS1*, a protein with anti-angiogenic activity (45, 46), shows significantly decreased expression (Figure 4). Iron uptake, heme, and myoglobin synthesis genes come up beginning in OCT with a spike in gene expression of transferrin receptor (*TFRC*), the rate-limiting enzyme in heme synthesis *ALAS1*, and myoglobin (*MB*) along with reduced expression of heme degradative enzymes *HMOX1*, *HMOX2*, and *POR*. The iron-sulfur cluster assembly enzyme (*ISCU*), mitochondrial iron transporter *SLC25A28*, the mitochondrial heme transporter *ABCB6*, the electron transfer flavoprotein-ubiquinone oxidoreductase (*ETFDH*), and the cytochrome c oxidase subunit *COX7A2L* are all upregulated during the hibernation season and are all involved in the production of heme and iron related proteins. Expression of the transcriptional coactivator implicit in a variety of mitochondrial function, PPARgamma coactivator-1alpha (*PPARGC1A*), peaks in OCT and returns to APR levels in TOR and IBA. The homologue PGC-1β (*PPARGC1B*) is expressed at peak levels during TOR and IBA. Each of these transcriptional coactivators have been

shown to promote expression of genes associated with increased oxidative capacity (47).

Functional Category	*Gene Name*	Normalized mRNA Reads			
		April	October	Torpor	IBA
TCA cycle	*IDH3A*	2697	5350	4433	4583
	ACO2	16448	24399	17987*	15593*
Promoting oxidative metabolism	*THRB*	67	91	106	121
	PPARGC1A	126	201	146*	175
	PPARGC1B	77	122	198*	204*
Angiogenesis	*VEGFA*	1660	2884	1746*	1748*
	VEGFB	1108	2172	1674*	1722
	ADAMTS1	258	128	21	75
Iron-sulfur cluster and heme synthesis	*TFRC*	194	2934	327*	308*
	ISCU	1144	1561	1993*	2205*
	ALAS1	854	2751	1017*	981*
	ALAS2	11	20	21	19
	HMOX1	383	67	446*	452*
	HMOX2	492	299	402*	366
	SLC25A28	147	158	240*	215
	ABCB6	898	900	1292	1225
Oxygen transport/reserve within cells	*MB*	64821	114017	87326*	99345
Mitochondrial ADP/ATP transporters	*SLC25A4*	33596	51613	59720	55883
	SLC25A6	2217	2465	3754	4251

Figure 4. Gene expression changes supporting an increase in oxidative capacity immediately preceding and during hibernation. Genes are grouped into functional categories based on their role in oxidative capacity. Differential expression relative to April is signified by red (increased expression) or green (decreased expression) shading. Differential expression relative to October is signified by an asterisk.

Muscle maintenance and regulation of protein turnover

Transcriptomic analysis reveals differential expression of genes involved in key pathways determining the rates of protein synthesis and degradation. Genes involved in protein synthesis, including the mTOR pathway show increased expression during the hibernation season. The key enzymes in this pathway that are upregulated are *AKT1*, *MTOR*, and *RPS6KB1* (Figure 5). Similarly, inhibitors of protein synthesis, *DDIT4*, *KLF1*5, and *EIF4EBP1* show decreased expression at the same time points. This

pathway is likely regulated through IGF signaling during hibernation, with *IGF1* and *IGF2* showing significant upregulation, while the inhibitory IGF binding proteins *IGFBP2* and *IGFBP7* are significantly downregulated. We also see evidence of reduced protein degradation during the hibernation season, including reduced expression of the negative regulator of muscle growth myostatin (*MSTN*), the transcription factors *FOXO1* and *FOXO3*, and the TWEAK receptor Fn14 (*TNFRSF12A*), which are all upstream activators of ubiquitin-mediated proteolysis (Figure 5).

Functional Category	*Gene Name*	Normalized mRNA Reads			
		April	October	Torpor	IBA
Protein Synthesis	*IGF1*	159	224	491*	288
	IGF2	87	148	165	179
	AKT1	552	872	897	866
	MTOR	1120	857	1569*	1272*
	RSPS6KB1	312	409	486	531*
Negative Regulation of Protein Synthesis	*DDIT4*	2073	508	66*	270
	KLF15	492	349	85*	167
	EIF4EBP1	227	168	150	185
	IGFBP2	105	51	17*	20*
	IGFBP7	525	395	370	335
	MSTN	111	32	11*	29
Protein Degradation	*FOXO1*	638	520	246*	249*
	FOXO3	810	651	334*	384*
	TNFRSF12A	357	130	46	75
	ZFAND5	2487	1246	1069	1158

Figure 5. Gene expression changes supporting a shift in protein turnover during hibernation. Genes are grouped into functional categories based on their role in protein turnover. Differential expression relative to April is signified by red (increased expression) or green (decreased expression) shading. Differential expression relative to October is signified by an asterisk.

Discussion

Skeletal muscle is a highly abundant and metabolically costly tissue. As such, it is expected that greater physiological transitions must occur to allow this tissue to endure the demands of hibernation. Similarly, any changes in skeletal muscle

physiology are likely to have body-wide consequences that could facilitate the hibernation phenotype. Using Illumina HiSeq sequencing technologies we were able to perform a high-throughput analysis of skeletal muscle gene expression at various time points throughout the circannual cycle of the thirteen-lined ground squirrel. This analysis improves on previous transcriptome analyses performed in our lab that relied on subtractive hybridization (48), EST identification (28), or 454 sequencing technologies that used pooled samples and therefore lacked statistical validation of expression levels at any given time point (32). The depth of coverage using these techniques allowed us to validate and expand on previously known physiological transitions, while also making some novel mechanistic hypotheses.

Fuel Utilization

During conditions in which whole-body metabolism changes, such as hibernation, the relative contribution of individual substrates to energy production will alter. For example, in rats fasted for 48 hours mRNA levels for glucose-handling proteins were reduced by as much as 70%, while transcripts involved in fatty acid transport and metabolism were increased over 50% (49). Because hibernation involves a long-term fast meant to conserve energy at a time of limited nutrient availability, we proposed that changes in gene expression similar to fasting are occurring during hibernation.

Fatty acid and glucose metabolism.

Mammalian hibernators rely almost exclusively on lipid reserves accumulated during summer and fall months, while carbohydrate utilization is drastically reduced (3). The switch from carbohydrate to fatty acid metabolism is regulated by differential gene expression at multiple levels and shares several gene expression changes with fasting

(50, 51), including increased expression of the acyl-CoA dehydrogenases *ACADS*, *ACADVL*, and *ACAD10*, and the mitochondrial transport protein *CPT1* (Figure 3). These similarities with fasting reflect the requirement for fatty acid transport and β-oxidation upon nutrient deprivation, and increased circulating fatty acid concentrations.

Key differences between fasting and hibernation, as evidenced by mRNA expression, come from the differences in fatty acid transport proteins. Increased expression of the fatty acid translocase *CD36* is observed in the skeletal muscle of fasting rats (50, 51), while elevated transcript levels of the fatty acid transport protein *SLC27A1* are observed during hibernation in ground squirrels. Studies have shown *SLC27A1* directs fatty acids for oxidation (52), is particularly effective at facilitating long-chain fatty acid transport (53), and is protective against intramuscular lipid accumulation (52). We postulate the increased expression of *SLC27A1* allows for increased ability to transport unsaturated fats across the membrane, and that this is a key difference between fasting and hibernation-associated fasting, given that unsaturated fats remain more liquid at cold temperatures. Taken together, fasting and hibernation-associated fasting both show similar upregulation of fatty acid metabolism, although differences in enzymes might reflect the greatly increased fat storage prior to hibernation that is not seen in normal fasting.

Oxidative capacity.

While many of the genes associated with β-oxidation show a gradual increase through OCT, peaking in hibernation, there is an OCT-specific increase in genes associated with oxygen delivery and transport, which would be necessary for the rapid utilization of these fats in oxidative phosphorylation. The primary method of iron uptake into muscle cells is through the binding of transferrin to transferrin-receptor, and its

subsequent endocytosis (54). Transferrin-receptor (*TFRC*) shows a 15-fold increase in OCT from APR, and then decreases, but is still differentially elevated during hibernation (Figure 4). Once iron is in the cell it can be stored in ferritin, transported back out of the cell, or incorporated into various functional proteins, usually in the form of heme (54). Increased transcriptional expression of the rate-limiting enzyme in heme synthesis, *ALAS1*, and decreased expression of heme-degradative enzymes, *HMOX1*, *HMOX2*, and *POR* indicate enhanced heme synthesis in OCT. In addition to the mitochondrial cytochromes, heme groups can be incorporated into the oxygen transport protein myoglobin (*MB*). In accordance with previous studies, our transcriptome shows significantly increased *MB* expression in OCT in skeletal muscle, with the protein product likely being maintained throughout hibernation (55). In diving mammals that undergo regular acute hypoxic events, *MB* is increased in their skeletal muscles as a means of buffering against anaerobic metabolism and the buildup of lactate (56). The increased MB expression in hibernators likely serves a similar purpose during the rewarming process associated with an IBA. Shivering thermogenesis is an important part of the rewarming process, during which, oxygen consumption can be as high as three times normal active levels (57). With such extreme whole-body oxygen demand, the muscles run the risk of using oxygen more rapidly than it can be delivered and resorting to anaerobic metabolism. The importance of remaining aerobic during rewarming is also highlighted in the significantly increased expression of the mitochondrial ADP/ATP transporters *SLC25A4* and *SLC25A6* during hibernation (Figure4) ,indicating an increased reliance on mitochondrial ATP generation. Finally, angiogenic factors *VEGFA* and *VEGFB* also show increased expression in OCT further, likely increasing capillary density and further preparing the animal for increased in oxygen demands (Figure 4).

These changes in oxidative capacity are likely mediated through differential expression of the transcriptional coactivators (TCs) *PPARGC1A* and *PPARGC1B*. These TCs are known to induce the expression of a wide variety of genes related to mitochondrial function, oxidative capacity, and the myosin fiber type transition observed in our data and others (58,59). The differential expression of these TCs correlates with their expected transcriptional targets in such a way to suggest that *PPARGC1A* is more responsible for the physiological transition into hibernation with peak expression in OCT, and *PPARGC1B* plays a role in maintaining the hibernation phenotype with increased expression during TOR and IBA. A role of *PPARGC1A* in hibernation has been recently proposed (23), and our data supports these findings, but further research is needed to determine the full role of *PPARGC1A* and the role of *PPARGC1B* in the hibernation phenotype.

Muscle Maintenance with Altered Protein Turnover

Under normal conditions, muscle homeostasis is achieved by balancing the continuous processes of protein synthesis and degradation. This balance is regulated by mechanisms integrating a variety of signals including nutrient availability and functional demand. Under conditions of fasting or immobility such as those seen in hibernation, these mechanisms can lead to severe muscle atrophy (60, 61). The amount of inactivity typical of a 10-day torpor bout would, in the non-hibernating rat, result in 16-27% reduction in muscle mass depending on muscle type (62). Hibernators interrupt these long periods of immobility only briefly during IBAs thus remaining largely immobile for 6 months. Throughout this time their muscles retain normal morphology and functionality (21). The high throughput transcriptome data provides a comprehensive view of potential regulatory points in the protein synthesis and degredative pathways that

hibernators may use to avoid atrophy. The atrophic response of non-hibernator skeletal muscle has been well characterized at the transcriptional level (15). A direct comparison of gene expression patterns of active (APR) versus hibernating (TOR) ground squirrels to active versus immobilized rats reveals a nearly complete lack of the typical atrophic response despite extended disuse in hibernation.

Studies suggest that transcription and translation are halted during torpor (8, 9), implying that the protein synthesis necessary to counteract protein degradation can only occur during an IBA. Our hibernators show increased expression of genes in the IGF-1/AKT/mTOR pathway, which is typical of the hypertrophic response to exercise (63) and is a central mechanism of activating protein synthesis. The increased transcriptional expression of the mTOR pathway and reduced expression of its inhibitors, such as *DDIT4* and *KLF15*, supports the hypothesis that protein synthesis may be occurring in bursts during the IBAs to counteract the processes of protein degradation, but further investigation at the level of proteins and post-translational regulation would be needed to confirm the role of this pathway (64). Mechanisms of protein degradation include the ubiquitin proteasome system, the lysosomal autophagy system, and Ca^{+2}-activated proteases (calpains). In models of disuse these pathways are upregulated, resulting in an unbalanced rate of protein turnover eventually leading to atrophy. Our transcriptome data shows most of these systems to have stable expression despite the conditions of disuse and fasting. However, many important transcription factors and signaling cascades that eventually lead to the activation of these systems show significantly reduced expression during hibernation.

The FOXO transcription factors are master regulators of a variety of proteolytic systems including the lysosomal autophagy system and the ubiquitin-mediated proteolysis system. AKT and the PGC-1 transcriptional coactivators are known to inhibit

FOXO transcriptional activity (65, 66). Their overexpression during hibernation could explain the steady expression of FOXO transcriptional targets despite conditions of immobility and fasting that should lead to their overexpression (60, 61). One such transcriptional target of FOXO transcription factors is the gene *ZFAND5*, which plays a major role in the recognition, delivery, and anchoring of ubiquinated proteins to the proteasome (67). *ZFAND5* shows significantly reduced expression beginning in OCT through the hibernation season (Figure 5), demonstrating direct regulation of the rate of protein degradation. NF-κB signaling is another important modulator of muscle atrophy (68). NF-κB activation by the proinflamitory cytokine, TNF-like weak inducer of apoptosis (TWEAK), has recently been demonstrated to contribute to the atrophic response by inducing the expression of MuRF1 and Atrogin-1, both E3 ubiquitin ligases. (69). Reduced expression of the TWEAK receptor *TNFRSF12A* suggests another method by which these animals reduce the rate of protein degradation during hibernation (Figure 5). Through transcriptional regulation at various levels, from major transcription factors to cytokines to proteasome anchoring proteins, these animals seem able to maintain a normal rate of protein turnover under otherwise atrophic conditions, and preserve muscle function and mass.

Conclusion

Overall, the depth of this type of data has allowed us to observe changes in gene expression never before quantified. This data has yielded information on how the physiological transitions in hibernator skeletal muscles might be contributing to the hibernation phenotype. The metabolic transitions we see at the gene expression level would allow their muscles to efficiently metabolize lipids, the primary fuel source during hibernation. Supporting this oxidative metabolism, we see increased expression of

oxygen delivering/handling genes just prior to hibernation. Finally, to avoid the effects of the extended disuse associated with hibernation, these animals show altered gene expression of a variety of genes key to protein balance.

Chapter 2: Proteome Analysis

Materials and Methods

Animal Models

Thirteen-lined ground squirrels (*Ictidomys tridecemlineatus*) used in this study were obtained and housed as described previously (70, 27). All experimental animal procedures were approved by the University of Minnesota Institutional Animal Care and Use Committee. The following collection points served to reveal changes in protein abundance throughout the circannual cycle: April Active (APR), August Active (AUG), October active (OCT), January torpor (TOR), January interbout arousal (J-IBA), and March interbout arousal (M-IBA) (Figure 1). Three females and three males were collected at each time point. A single female sample and a single male sample were eventually pooled to produce three samples comprising both sexes. Three mass spectrometry runs were performed on iTRAQ labeled samples with each including one sample from each of the six time points. This resulted in a total of three biological replicates for each time point. Physiological state was determined by rectal temperature and animal behavior. At all time points, animals were anesthetized with isoflourane and sacrificed by decapitation. The quadriceps muscles were dissected and immediately frozen in liquid nitrogen and stored at -80°C. Animals collected for all time points, except TOR, had a body temperature (T_b) of 35-37°C and were observed as being fully awake and active prior to sacrifice. Torpid animals were collected after a minimum of three days of consecutive torpor, showed no outward signs of arousal, and had a T_b of 5-7°C at the time of sacrifice.

Protein Extraction and iTRAQ labeling

Frozen tissue was ground to a powder under liquid nitrogen. Tissue was reconstituted in extraction buffer (7M urea, 2M thiourea, 0.4M triethylammonium bicarbonate (TEAB) pH8.5, 20% acetonitrile, and 4mM Tris (2carboxyethyl) phosphine (TCEP)) at a ratio of 10ml/g. While remaining on ice, the samples were sonicated with a Branson Digital Sonifier 250 at 30% amplitude for no more than 7 consecutive seconds to avoid carbamylation. A volume of 150µl of each sample was transferred to a Pressure Cycling Technology tube and capped with a 150µl cap before being placed in the Barocycler NEP2320 (Pressure Biosciences, Inc., South Easton, MA). Samples underwent 40 cycles of 35 kpsi for 30 seconds followed by 0 psi for 15 seconds. Following pressure cycling, 200mM methyl methanethiosulfonate (MMTS) was added to a final concentration of 8mM, mixed, and incubated at room temperature for 15 minutes. Samples were then transferred to a new 1.5ml microfuge Eppendorf Protein LoBind tube. Protein concentration was determined by Bradford assay.

Protein from a single male and a single female (50µg each) were pooled to produce samples of 100µg. This was brought up to a least common volume in protein extraction buffer and MMTS. Samples were diluted 4-fold with ultrapure water followed by the addition of trypsin (Promega, Madison WI) at a ratio of 35:1 total protein to trypsin. Samples were incubated at 37°C for 16 hours and then frozen at -80°C for 30 minutes prior to drying by vacuum centrifugation. After cleaning the samples using normal phase solid phase extraction (SPE) (Extract CleanTM C18 SPE cartridge, Grace-Davidson, Deerfield IL), the eluents were vacuum dried and resuspended in dissolution buffer (0.5M TEAB pH8.5) to a final concentration of 2µg/µl. iTRAQ® labeling was done

per manufacturer's protocol (AB Sciex, Foster City CA). After labeling, samples were multiplexed and vacuum-dried. Samples were cleaned by normal phase SPE as before and eluents were dried by vacuum centrifuge.

Liquid Chromatography Fractionation and Mass Spectrometry

Labeled samples were resuspended in Buffer A (20mM ammonium formate pH=10 in 98:2 water:acetonitrile) and fractionated offline by high pH C18 reverse-phase chromatography (71). A Shimadzu Promenance HPLC (Shimadzu, Columbia MD) was used with a C18 XBridge column, 150mm × 2.1mm internal diameter, 5µm particle size (Walters Corporation, Milford MA). Flow rate was 200µl/min with a gradient from 2-35% Buffer B (20mM ammonium formate pH=10 in 10:90 water:acetonitrile) over 60 minutes followed by 35-60% over 5 minutes. Fractions were collected every 2 minutes and UV absorbances were monitored at 215nm and 280nm. Peptide-containing fractions were divided into early and late groups, each containing an equal number of fractions. The first early fraction was concatenated with the first late fraction and so on. Concatenated samples were dried by vacuum centrifugation, resuspended in load solvent (98:2:0.01 water:acetonitrile:formic acid) and 1-1.5µg aliquots were run on a Velos Orbitrap mass spectrometer (Thermo Fisher Scientific Inc., Waltham MA) as described previously with the exception that the higher-energy collisional dissociation activation energy was 20ms.

Bioinformatic Analysis

MS/MS spectra were searched using a customized ground squirrel database (70). This database was generated using predicted protein sequences from the NCBI annotated genome for the thirteen-lined ground squirrel, RNAseq data generated in this lab (27), and a contaminants database (cRAP) containing common or unavoidable MS

protein contaminants. Databases were merged using tools within the Galaxy-P platform (University of Minnesota) and searched using Paragon Algorithm (V.4.5.0.0) search engine in Protein Pilot (V.4.5, Sciex, Foster City CA) with the following search parameters: Sample Type: iTRAQ 8-plex (peptide labeled); Cys-alkylation: MMTS; Instrument: Orbi MS, Orbi MS/MS; Run Quant; Use bias correction; Search focus on biological modifications; Thorough search and with a Detected Protein Threshold (Unused Protscore (Conf)): 10%. The ProteinPilot searches and subsequent generation of PSPEP (FDR) reports and protein and peptide-level summaries were generated within Galaxy-P.

All peptides were identified with at least a 95% confidence interval value as specified by the Paragon Algorithm and less than a 1% false discovery rate (FDR) based on forward and reverse searches. Proteins were considered confidently identified with at least 2 unique peptides and an experiment-wide FDR of no more than 2%. Relative quantification of proteins was determined by ProteinPilot. ProteinPilot begins quantitation at the level of the peptide by calculating a ratio of any 2 iTRAQ label peak intensities (Figure 6). Ratios from all peptides matching a specific protein are then integrated to provide quantitative information for the protein. Comparisons were done between consecutive time points throughout the circannual cycle (Figure 1). A quantitative false discovery rate (FDR) of 2% was set by assigning a p-value threshold using the target-decoy method provided in the ProteinPilot Descriptive Statistics Template (Sciex, Foster City CA). The target-decoy method utilizes technical replicates (Figure 6) within a single MS/MS experiment to determine a p-value at which identical samples show an acceptable amount of difference (FDR of 2%). Based on this established FDR, proteins were considered differentially expressed within a single replicate if they had a p-value of less than .05 for the first and third replicates, and a p-

value below .001 for the second replicate. Because there is no standard method for averaging ratios and combining p-values across multiple MS runs, we considered protein abundances to be significantly different (using all three replicates) if at least two of the three replicates showed significance as stated above and showed a similar change in abundance (upregulated or downregulated). Proteins that showed differential expression in conflicting directions were not used for further analysis. Protein lists were submitted to DAVID for broad functional analysis.

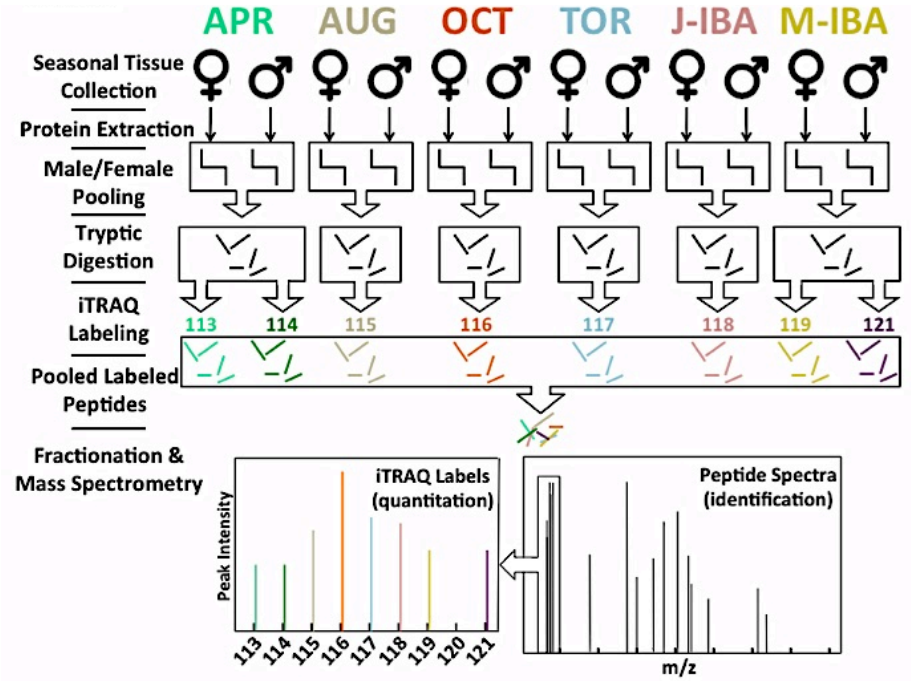

Figure 6. Sampling design, preparation, and iTRAQ labeling. Protein was extracted from male and female thirteen-lined ground squirrel quadriceps for each collection point. Equal amounts of protein were combined from one male and one female before tryptic digestion. The resulting peptides were iTRAQ labeled and all samples were pooled for mass spectrometry analysis. This illustration depicts a single mass spec run, representing a single biological replicate for each collection point with technical replicates made from the APR and M-IBA samples. This process was performed three times for a total of three biological replicates.

The identification of peptides corresponding to potential novel proteoforms was done largely using the platform Galaxy-P. Galaxy-P was used to filter out all peptides matching to known protein sequences from ground squirrel encoded by the NCBI

genome. The remaining peptides, identified from RNAseq data, were filtered using BLAST-P to search against the NCBI thirteen-lined ground squirrel non-redundant database. Identifications made by BLAST-P were further filtered to account for percent of identical amino acids, number of gaps in query, and length of the query relative to the input. Resulting peptides were searched against the NCBI human database. Novel peptides identified from this process were checked for high quality spectral matches using a Peptide Sequence Match Evaluator tool in Galaxy-P and the protein sequences were aligned to ground squirrel and human sequences to visualize how the novel peptide differed from the known or predicted sequences (70). The workflows used in this study have been described in details in proteogenomic study of saliva (72).

Results and Discussion

The role of skeletal muscle plasticity in the life cycle of a hibernator.

The goal of this experiment was to identify proteomic transitions occurring in skeletal muscle that might explain certain tissue-specific and whole-body physiological transitions observed throughout the circannual cycle of this hibernator. An earlier study in our lab developed a proteomic approach to identify proteins from non-model organisms that also used the thirteen-lined ground squirrel (73). In this study we employed iTRAQ-based tandem mass spectrometry (MS/MS) techniques to determine relative protein levels at 6 points throughout the year (Figure 1). In MS/MS runs 1, 2, and 3 respectively there were 36,895, 40,833, and 34,813 spectra matched to peptide sequences. These spectra were used to identify 15,229, 16,586, and 16,753 distinct peptides. After searching these peptides against the NCBI predicted protein database for the ground squirrel, our own database generated from high-throughput RNA-seq

data, and a contaminant database, we identified 1,055, 1,335, and 1,219 proteins across three separate MS/MS runs. Together, 1,563 proteins were confidently identified. For differential expression analysis, we made comparisons between sequential collection points (Figure 1). Across all comparisons, 232 proteins met our criteria for differential expression (see Methods). This approach recently identified a similar number of differentially expressed proteins in thirteen-lined ground squirrel hearts (70). These 232 proteins were then functionally clustered using DAVID. Categories indicated by DAVID are consistent with previously described physiological transitions for hibernator skeletal muscle, such as changes in metabolic preference and fiber type (Figure 7) (22, 23, 27, 74).

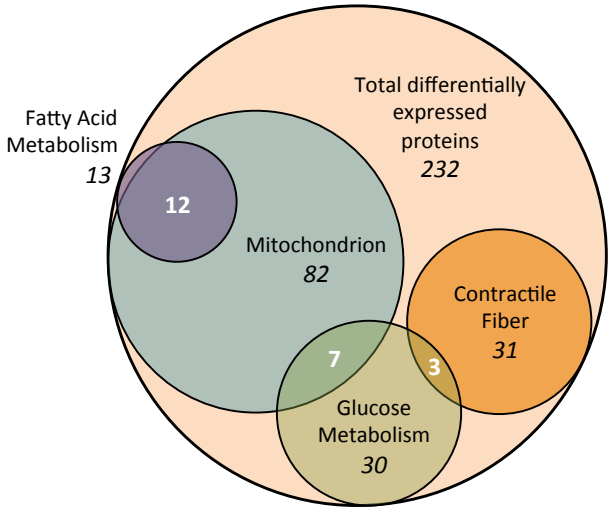

Figure 7. Major categorizations made by DAVID analysis of all differentially expressed proteins. Total number of proteins in a given category is represented with black numbers, whereas proteins shared between two categories are represented with white numbers.

Metabolic Transitions

The most notable transitions in protein abundance are consistent with previous findings that fatty acid oxidation is enhanced and glucose metabolism is reduced during the hibernation season in skeletal muscle (2, 3). The comparison with the largest

number of differentially expressed proteins was between M-IBA and APR, with 184 proteins. Despite the fact that these collection points are less than a month apart, this comparison has almost three times as many differentially expressed proteins than any other comparison. This supports the idea that the transition into the hibernation phenotype is a gradual one, occurring throughout the summer and fall, whereas the transition out of hibernation to an active and fed state is much more abrupt. The most notable fluctuations in metabolic proteins also occurred between the M-IBA and APR collection-points (Figure 8). Relative to M-IBA, proteins related to glucose metabolism increase sharply, while fatty acid metabolism proteins decline at the APR collection point. During their final spring arousal, occurring between M-IBA and APR, the animals have access to carbohydrates for the first time in nearly six months. Thus, an increase in the enzymatic machinery necessary to derive energy from this new fuel source is important as they are recovering from the previous hibernation season and preparing for reproduction. Alternatively, the transition to efficiently metabolizing fatty acids is a more gradual. Proteins involved in fatty acid metabolism consistently have a positive ratio, indicating a gradual increase in abundance throughout most of the year (Figure 8). Similarly, proteins involved in glucose metabolism tend to have a negative ratio at the same comparisons, indicating a gradual decline.

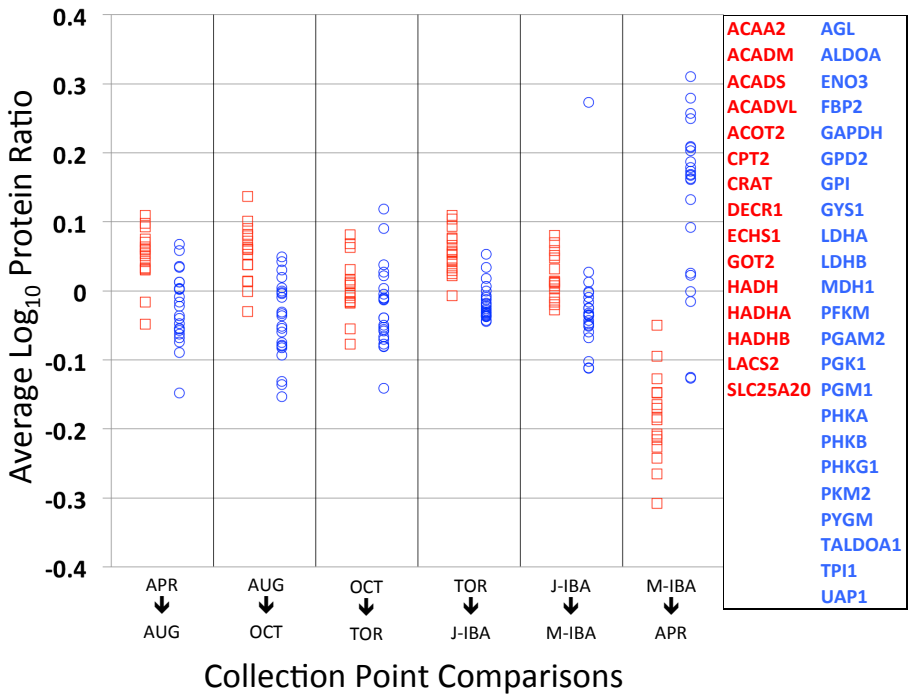

Figure 8. Abundance profile of metabolism-related proteins. All expression profiles charted are of proteins that are differentially expressed in at least one comparison. Red squares represent proteins involved in fatty acid metabolism. Blue circles represent proteins involved in glucose metabolism. Positive and negative ratios indicate an increase or decrease in protein abundance, respectively, from one time point to the next.

The comparison with the fewest differentially expressed proteins is TOR to J-IBA with 24 proteins. Because translation does not occur at T_b associated with TOR, IBAs are thought to be necessary for the production of proteins essential to the continuation of the hibernation phenotype (8, 9). The majority of proteins with increased abundance at this comparison are related to β-oxidation (HADHA, HADHB), the TCA cycle (FH, MDH1, SUCLA2, IDH3A, CS), and ATP synthesis (ATP5A1 and ATP5B). This reflects both the reliance of hibernating animals on fatty acid oxidation for making ATP, as well as the importance of the IBAs for replenishing necessary proteins. In summary, these data provide valuable insight into the rate and timing of metabolic transitions occurring in the skeletal muscle of these hibernators.

Fiber-type transitions

Associated with these transitions in metabolic properties, we also see shifts in contractile proteins throughout the circannual cycle. Figure 9 shows the abundance of contractile proteins classified as fast-twitch, slow-twitch, or non-specific isoforms. It should be pointed out that myosins compose as much as 50% of the total protein of skeletal muscles and exist as either fast or slow isoforms, so major shifts in these proteins will have a larger effect on muscle mass than others (75). As with metabolism, the most abrupt transition occurs between the M-IBA and APR collection points, with increases in fast-twitch associated isoforms and a reduction in slow-twitch isoforms. This correlates with the fact that fast-twitch muscles use a more glycolytic metabolism and that these animals' muscles grow significantly upon spring re-feeding (26). In contrast to the metabolic fluctuations, where we saw a gradual return to the hibernation phenotype, the contractile proteins show a much more variable expression pattern, reflecting both changes in fiber-type abundance and overall muscle mass. APR to AUG shows an increase in muscle mass with increases in slow fiber types. AUG to OCT, a period where these animals are greatly reducing their food intake and using shallow torpor bouts with increasing frequency (76, 6), shows a reduction in both fiber types, likely indicating a reduction in muscle mass between these points. Fiber-type composition tends not to change through early hibernation, but shows a surprising increase in abundance of slow-type isoforms between the J-IBA and M-IBA collection points. This transition supports a recent study demonstrating a re-investment in muscle protein synthesis in preparation for spring arousal (26). These data suggest that these animals are actively growing muscle at a time when they have not eaten for at least 3

months and are mostly sedentary except for shivering thermogenesis and limited movement during IBAs.

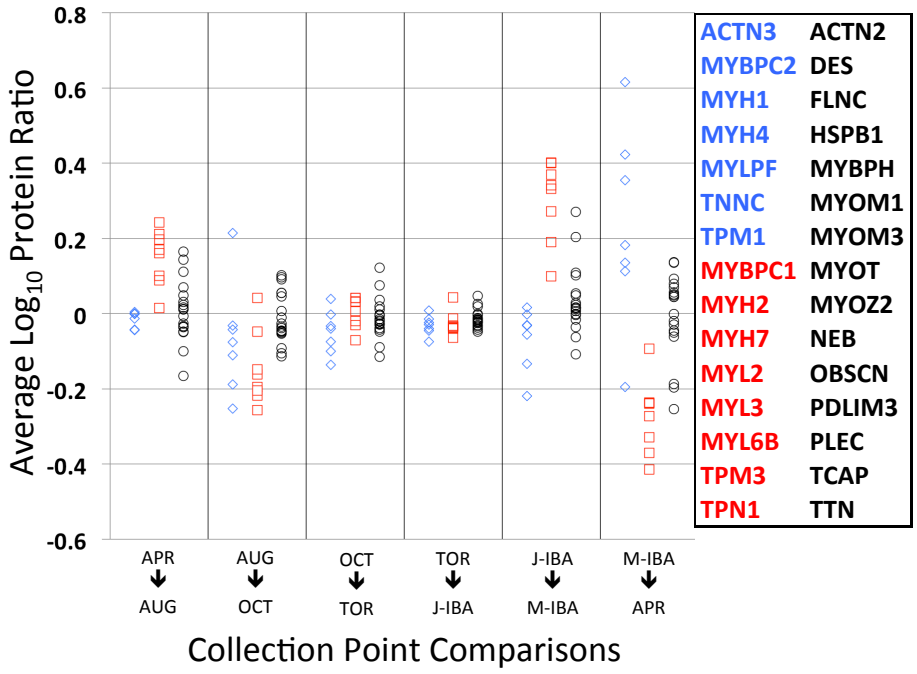

Figure 9. Abundance profile of contractile/structural proteins. All profiles charted are of proteins that are differentially expressed in at least one comparison. Blue diamonds represent protein isoforms consistent with a fast-type muscle. Red squares represent protein isoforms consistent with a slow-type muscle. Black circles represent proteins without specific fast or slow isoform types.

Potential roles of AMP Deaminase 1

The high abundance and metabolic demand of skeletal muscle necessitates the use of a strong negative feedback system in which this tissue can maintain energy balance in response to fluctuating energy demand and availability. The AMP:ATP ratio serves as a major signal of cellular energy status. During periods of high ATP utilization, this ratio is elevated (77, 78). High AMP:ATP promotes the phosphorylation and activation of AMP-activated protein kinase (AMPK) which signals downstream processes aimed at increasing ATP production and decreasing ATP utilization (79). In response to acute energy deficit, AMPK maintains energy homeostasis through inhibiting protein

synthesis and enhancing glucose and fatty acid uptake and utilization (79). For a more chronic energy deficit, AMPK has been implicated in increasing mitochondrial biogenesis through increased activity and activation of PGC-1α, a transcriptional co-activator differentially expressed and activated during hibernation (27, 80-82). A major regulator of the AMP:ATP ratio identified as being differentially expressed in our proteome is the protein AMP deaminase 1 (AMPD1) (Figure 7). AMPD1 catalyzes a rate limiting reaction in the main catabolic pathway of AMP to IMP, thus its reduction would promote a higher AMP:ATP ratio during periods of rapid ATP hydrolysis (83). These data demonstrate that the abundance of AMPD1 is significantly reduced preceding and during hibernation (Figure 10). This reduced ability to clear cellular AMP could lead to increased AMPK activity, especially during periods of muscle activity, which could induce many of the physiological transitions associated with hibernation including increased mitochondrial protein density (Figures 8 & 11), increased fatty acid metabolism (Figure 8) (2, 3), reduced muscle mass (26), and the fast to slow fiber-type transition (Figure 9) (22), all of which occur at times congruent with reduced AMPD1 abundance.

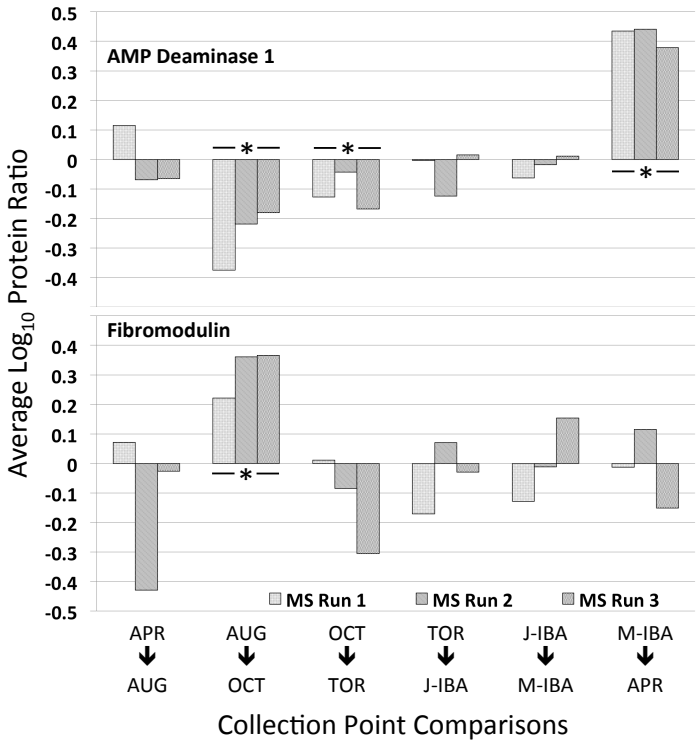

Figure 10. Relative protein abundance of AMPD1 and FMOD for 6 comparisons made throughout the circannual cycle. Ratios for each mass spec run are represented independently, with an asterisk indicating comparisons that fit our criteria for differential expression. AMP-deaminase 1 (AMPD1) shows significantly reduced abundance from AUG to OCT and from OCT to TOR, while showing significantly increased abundance from M-IBA to APR. Fibromodulin (FMOD) has significantly increased abundance from AUG to OCT without any clear decrease, likely indicating a gradual decline, never showing significance.

Additionally, this decrease in AMPD1 during hibernation could reflect an alteration in the production of nitrogenous waste. During intense exercise, AMP is deaminated to IMP as a way of pulling the reaction catalyzed by adenylate kinase in the direction of making more ATP. As a consequence, tissue and blood levels of ammonia increase shortly after beginning exercise, reflecting this breakdown of AMP (84, 85). Human individuals can, asymptomatically, be heterozygous or homozygous for a mutation in AMPD1 that renders it catalytically inactive. Interestingly, these individuals show no increase in blood ammonia during or after exercise (85). The reduced adenylate degradation in these individuals significantly reduces the amount of ammonia

waste they produce during exercise. These hibernators drink and urinate little, if at all, for the length of the hibernation season, yet periodically need to activate their muscles to a high degree for shivering thermogenesis (55). Reducing the amount of nitrogenous waste produced during these exercise bouts greatly limits the amount of urine they need to produce.

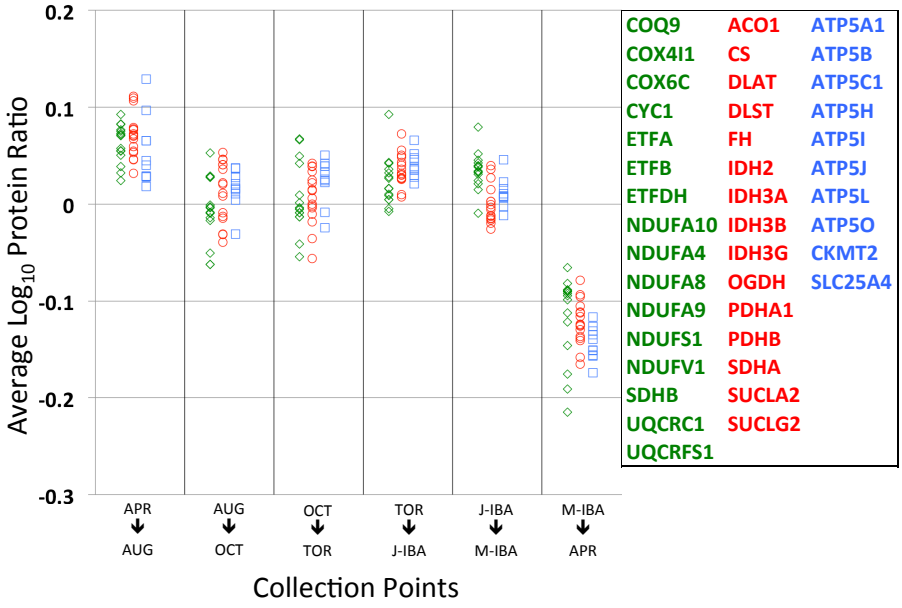

Figure 11. Abundance profile of mitochondrial proteins. Excludes metabolism proteins already shown in Figure 4. All profiles charted are of proteins that are differentially expressed in at least one comparison. Green diamonds represent proteins associated with the electron transfer system. Red circles represent proteins involved in the TCA cycle. Blue squares represent proteins closely associated with ATP production, most of which are subunits of ATP synthase.

Finally, reduced ability to clear cellular AMP may have another very active role in hibernation. With reduced ability to deaminate AMP to IMP, an alternate degradative pathway involves hydrolyzing AMP to adenosine (84). During periods of high ATP utilization, such as shivering thermogenesis for IBAs, levels of muscle AMP and adenosine would be expected to spike (84). Our previous work has shown that the transcript for the equilibrative nucleoside transporter 1 (*SLC29A1*) has significantly

elevated expression during hibernation (27). This transporter might allow the release of excess adenosine from the skeletal muscle into circulation (86). Circulating adenosine has long been suspected as a major signal in the torpor-arousal cycle since it was demonstrated that adenine nucleotides or adenosine injections induce a hypometabolic state in mice with similarities to fasted daily torpor (87, 88). Tissue specific targets of adenosine might include the deactivation of non-shivering thermogenesis in brown adipose tissue (BAT). Previous work in our lab has shown an increase in the transcript of adenosine receptor ADORA1 in BAT during hibernation, the activation of which could shut down adenylate cyclase activity and the subsequent metabolism of fatty acids necessary for heat production (35). This would represent a signaling mechanism between the two main tissues responsible for rewarming to and maintenance of a normal euthermic T_b. As BAT produces heat in the initial phase of rewarming, it warms the muscles to the point that they can begin shivering thermogenesis. Because of the low levels of AMPD1, there would be greater potential to produce adenosine, which could enter circulation and activate ADORA1 in BAT. This would slow heat production in BAT as the animal reaches the desired T_b.

Further studies are underway to determine the role of AMPD1 in AMPK activation, reducing nitrogenous waste, and the potential effects on circulating adenylate levels, especially surrounding the intense shivering thermogenesis associated with rewarming.

Fibromodulin helps maintain myogenic potential in myoblasts

Hibernator skeletal muscles have demonstrated delayed muscle regeneration during hibernation (89). Interestingly, they delay regeneration without suffering increased fibrosis as would happen in a typical mammal (89, 90). Andres-Mateos et al. (2012) suggested that reduced levels of transforming growth factor-β (TGF- β) likely

contribute to this phenomenon. TGF- β is a cytokine that is synthesized as an inactive complex that must be cleaved in the extracellular matrix (ECM) before binding to its receptor on the cell surface (90). During myogenesis, its signaling determines the differentiation of fiber types, while inhibiting muscle regeneration in adult muscle (91). TGF-β signaling is thought to be involved in the inflammatory response to muscle damage, but persistent signaling will cause myogenic cells to differentiate into fibrotic cells instead of new muscle (91). Various proteins of the ECM control TGF-β signaling by regulating cleavage to its active form or by sequestering it in the ECM to reduce its bioavailability (92-95). One such protein, fibromodulin (FMOD), increases significantly between AUG and OCT without a clear decrease, indicating a likely gradual decline in abundance through the rest of the year (Figure 10). FMOD is known to bind and maintain both the active and inactive forms of TGF-β in the ECM, limiting its bioavailability (94). Interestingly, it has also been shown play a role in the scarless repair of fetal skin (95). Its role in hibernator skeletal muscle could be similar, with increased levels modulating TGF-β signaling, allowing for more of a fetal response to muscle damage, resulting in muscle regeneration instead of fibrosis. Further evidence for this mechanism presented in this paper is the increase in slow-type protein isoforms expressed late in the hibernation season. If there were a period of muscle growth occurring late in hibernation, within this fetal-like ECM, it is expected that gene and protein expression would reflect a slow-type muscle (Figure 9) (90). Because of TGF-β's extensive roles in cellular growth and development, regulation of its signaling through increased abundance of FMOD could play a significant role in the muscle maintenance seen during hibernation.

Multi-omics analysis to improve genomic annotation

Collection and analysis of high throughput proteomic and RNAseq data from the same samples allowed us to identify specific amino acid sequences different from those predicted by automated genomic annotation. This proteogenomic method has proven particularly useful in non-model organisms, where genome annotation is typically less than ideal (27). Mass spectrometry runs 1, 2, and 3 identified 220, 214, and 241 peptides corresponding to novel proteoforms respectively with greater than 95% confidence. Two hundred and ten novel peptides were identified in two or more runs, with 99 being identified in all three runs. These 210 novel peptides represent 89 different proteins. This demonstrates the advantage of constructing a translated RNAseq database for proteomic analysis, as these peptides would have otherwise been unidentified. As previously reported in the ground squirrel heart, the majority of these peptides corresponding to novel proteoforms arise due to poor annotation of the genome (27, 96). There were 77 peptides identified for 17 proteins that had no genomic prediction. Additionally, 16, 14, and 27 peptides were identified that, when also aligned to the human protein, exist before the predicted start site, after the predicted stop site, or within unpredicted exonic regions, respectively.

Other peptides were identified that had a specific number of amino acids different from the predicted protein. Seventeen peptides had 10 or more residues different from the predicted, likely indicating problems with genome annotation or new protein isoforms. Another 17 peptides had 6-9 amino acid differences from the predicted, representing proteins with high biological variability, or poor annotation. Fifteen peptides had 2-5 differences form the predicted, while 24 peptides differed from their predicted

sequence by a single amino acid, likely representing sequence variability between the populations used for genomic sequencing and those used in this study.

Proteome/Transcriptome comparison

Another advantage to having both transcriptomic and proteomic screens from identical samples is the ability to interrogate basic biological questions such as the correlation between mRNA and protein abundance, and the type of regulation that may be occurring at different points in the circannual cycle. As in previous studies, this data highlights the unreliability of transcriptomic data to predict protein abundance (97). Of the differentially expressed transcripts that were also identified in the proteome, only 3.5 to 21.4 percent of them shared a similar expression pattern with their respective protein (Figure 12). This demonstrates a high degree of posttranscriptional regulation in determining protein levels.

Our data also indicate that the level of posttranscriptional regulation may vary according to season or physiological transition. Although a similar number of differentially expressed transcripts were identified in the proteome in the Oct:Tor and IBA:Apr comparisons, the percentage of transcripts matching their respective protein abundance more than double in the latter comparison (Figure 12). This may indicate an increase in posttranscriptional regulation leading up to the hibernation season, and a release from it following hibernation.

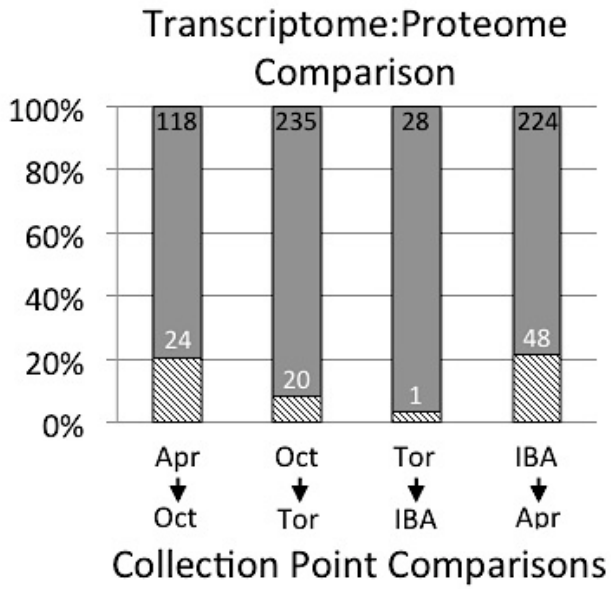

Figure 12. Differentially expressed transcripts and their protein products. Total number of differentially expressed transcripts with protein products identified in the proteome are indicated by the black numbers at the top of each bar. Total number of those proteins that show differential abundances similar to their respective transcripts are indicated by the white numbers, with the hatched bars indicating the percent of differentially expressed transcripts.

In conclusion, multi-omics approaches offer a major advantage, especially to the study of non-model systems where genomic information may be sparse or inaccurate. While the depth of coverage in high-throughput proteomics is not yet to the level of transcriptomics, the disparities between the two and the higher biological relevance of protein data make it a valuable tool not only for testing specific hypotheses, but for the generation of new hypotheses, as was the goal of this study.

Chapter 3: Future Directions--SERCA Efficiency

Materials and Methods

Animal Models and tissue collections

Thirteen-lined ground squirrels (*Ictidomys tridecemlineatus*) used in this study were obtained and housed as described previously (27, 70). All experimental animal procedures were approved by the University of Minnesota Institutional Animal Care and Use Committee. Samples were taken at two points throughout the year: during hibernation (HIB) and in the spring (APR). Because this was a pilot study and no data suggests any difference between TOR and IBA, HIB animals were taken regardless of state with 2 in TOR and 6 in IBA. Over all, 5 males and 3 females were taken during HIB and 5 males and 3 females were taken in APR. APR animals were taken out of the hibernation chamber, placed at 22°C on a 12:12 light:dark cycle and given food ad libitum for a minimum of 10 days before being sacrificed. At all time points, animals were anesthetized with isoflourane and sacrificed by decapitation. Muscle groups were dissected out, cleared of connective tissue and other debris, and placed immediately into ice-cold homogenization buffer (⊙).

Sarco-endoplasmic reticulum isolation

The ratio of calcium ions that are pumped per each ATP hydrolyzed by SERCA is its coupling ratio, and is a direct measure of SERCA efficiency. This ratio controls the metabolic demand of SERCA activity and is an indirect measure of the amount of heat SERCA is producing. To determine this coupling ratio, sarcoplasmic reticular vesicles first needed to be isolated to reduce potential activity of non-specific ATPases or calcium

sequestering mechanisms. Skeletal muscles were first minced with scissors in 5ml of homogenization buffer. Minced muscles were homogenized by three 15-second bursts with the TissueTearor tissue homogenizer resting 30 seconds on ice between each burst. The homogenate was filtered through 4 layers of gauze. Five ml of homogenization buffer was used to rinse extra homogenate from the homogenization tube and collection beaker. This was then centrifuged at 2,000×g for 10 minutes to pellet cellular debris. The supernatant was again centrifuged at 10,000×g to pellet mitochondria. Potassium chloride was added to the post-mitochondrial supernatant to a concentration of 0.6M (4.5g per 100ml). This was incubated on ice with gentle agitation for 30 minutes to solubilize the myosin globulins. The samples were then centrifuged at 40,000×g to pellet the sarco-endoplasmic reticular vessicles. This pellet was resuspended in 250ul of resuspension buffer (⬥) by repeated pipetting. Protein concentration was determined by BCA analysis.

SERCA efficiency assay

The coupling ratio of SERCA was determined using isolated SR vesicles and an ion-selective calcium electrode (WPI). Isolated SR vesicles were diluted to a concentration of 2mg/ml. The reaction chamber was a Hansatech Oxytherm with stir speed set to 75rpm and chamber temperature to 37°C. All measurements were performed in a 500µl reaction volume, consisting of 415µl of reaction buffer (★) and 85µl of isolated SR in resuspension buffer. Once chamber temperature was stabilized, stepwise additions of 5mM CaCl were made in the order: 1µl, 1µl, 2µl, 4µl, 8µl, allowing the reading to equilibrate after each addition. These additions set up a standard curve for determining calcium concentrations after ATP additions. After reaching a final calcium concentration of 160µM, 10mM ATP was added to a final concentration of 20 or

40μM depending on the anticipated calcium uptake response. This uptake caused a reduction in the calcium concentration of the solution read by the electrode. Readings were again allowed to equilibrate after each addition. Equivalent additions were made until the reading from the calcium electrode was outside of the range of the standards. ATP additions with a calcium concentration that remained above 20μM were used to calculate SERCA coupling ratio. This ratio was determined by first plotting the log of the known calcium concentration against the mV reading from the calcium electrode. The equation for the line of best fitting these points was then used to calculate calcium concentration from mV readings taken after ATP additions. The SERCA coupling ratio was calculated as moles of calcium removed from solution per mole of ATP added.

Tricine SDS-PAGE Western blot analysis

SR vesicles not used in the efficiency assay were again pelleted at 40,000×g. The SR pellet was resuspended in 200μl RIPA lysis buffer (⌘) and fully dissolved by syringe homogenization (25 gauge). Protein concentration was determined by BCA analysis. Samples were diluted with RIPA and then Tricine sample buffer (for SLN detection) or Laemmli sample buffer (for SERCA detection) to a final concentration of 2mg/ml. For SLN, 30μg of protein were run on a 16% separating gel (□) with a 4% stacking gel (#) optimized for Tricine samples. For SERCA, 5μg of protein were run on a 12% separating gel (@) with a 4% stacking gel ($). Separate anode (✜) and cathode (■) buffers were required for tricine SDS-PAGE. For Tricine gels, the voltage was set at 20V until the samples completely entered the stacking gel at which point the voltage was increased to 90V until the loading dye was ~2/3 down the gel. For

Laemmli gels voltage was set at a constant 190V until the loading dye ran off the bottom of the gel.

Protein was transferred to a .2μm nitrocellulose membrane in a wet transfer system. Both Tricine and Laemmli methods used the same transfer buffer (&). Voltage was set at 75V for 2.5-3 hours. Primary antibodies were used at recommended concentrations (1:1000 dilution) to detect SERCA1 (Abcam, ab105172) and SLN (Millipore, ABT13). Secondary antibody with conjugated HRP (1:6000 dilution) and SuperSignal West Pico chemiluminescent substrate were used for visualization.

Reagents

(⊙) Homogenization buffer:

- 10mM sodium bicarbonate
- 2mM sodium azide
- 10mM Tris-Cl
- pH 7.5

(♦) Resuspension buffer:

- 10mM Tris-Cl
- pH 6.0

(★) Reaction buffer:

- 100mM KCl
- 4mM $MgCl_2$
- 5mM sodium azide
- 5mM potassium oxalate
- 20mM Tris-Cl
- pH 6.0

(⌘) RIPA lysis buffer:

- 150mM sodium chloride
- 5mM EDTA
- 50mM Tris
- 1.0% Triton-X
- 10% sodium deoxycholate
- 10% SDS
- water up to 100ml (pH 8.0)

(□) 16% resolving gel (Tricine) (minigel system):

Mix 3ml AB-3 (❖), 3ml gel buffer (✪), 714µl glycerol, and 3.286ml water. To begin polymerization add 50µl 10% ammonium persulfate and 5µl TEMED. Pipette into gel casting set-up. Cover with a layer of isopropanol. Allow about 1hr to polymerize. Makes enough for 2 gels.

(#) 4% stacking gel (Tricine) (minigel system):

Mix 1ml AB-3, 3ml gel buffer, and 8ml water. To begin polymerization add 90µl 10% ammonium persulfate and 9µl TEMED. Pipette into gel casting set-up on top of rinsed and dried resolving gel. Insert well comb and allow about 30min to polymerize. Makes enough for 2 gels.

(@) 12% resolving gel (Laemmli) (minigel system)

Mix 3ml water, 4.34ml 40% acrylamide, 2.5ml 1M Tris pH 8.8, 100ml 10% SDS. To begin polymerization, add 5µl TEMED and 50µl 10% APS. Pipette into gel casting set-up. Cover with a layer of isopropanol. Allow 30min to polymerize.

($) 4% stacking gel (Laemmli) (minigel system)

Mix 3.82ml water, 0.5ml 40% acrylamide, 0.63ml 1M Tris pH 6.8, 50ml 10% SDS. To begin polymerization, add 5µl TEMED and 25µl 10% APS. Pipette into gel casting set-up. Insert well comb and allow 30min to polymerize.

(&) 10X Transfer Buffer

- 250mM Tris-Base
- 1.9M Glycine
- up to 1L with water

1X Transfer Buffer

- 100ml 10X transfer buffer
- 200ml methanol
- up to 1L with water
- good practice to make with enough time to chill in freezer before use

(❖) AB-3:

Dissolve 48g acrylamide and 1.5g bisacrylamide up to 100ml in water. Acrylamide is a potent neurotoxin, scoop into tared 50ml conical in the hood and move to balance to measure.

(✚) Tricine sample buffer (4X):

- 12% SDS (w/v)
- 6% mercaptoethanol (v/v)
- 0.05% coomassie blue
- 30% glycerol (w/v)
- 150mM Tris/HCl
- water up to 25ml (pH 7.0)

(✪) Gel buffer:

- 3M Tris
- 1M HCl
- 0.3% SDS
- pH 8.45

(✜) Anode buffer (10X):

- 1M Tris
- 0.225M HCl
- pH 8.9

(■) Cathode buffer (10X):

- 1M Tris
- 1M Tricine
- 1% SDS
- pH should be around 8.25, but do not adjust

Results and Discussion

Overview

In the transcriptomic and proteomic screens, genes and proteins involved in calcium handling were always readily identified because of their high abundance in skeletal muscle. We also see that many of these genes and proteins are differentially expressed, such that expression of these products tends to be depressed during hibernation. Thus, the goal of this project was to determine the consequences of this altered expression as it relates to calcium handling efficiency. Because calcium handling in skeletal muscle is such an energetically expensive process and because it can play a significant role in thermogenesis, the efficiency of the SERCA pump is likely to change in accordance with metabolic and thermoregulatory demands. While there are well-established methods to measure the kinetics of SERCA, no assay has yet attempted to directly measure the coupling ratio, or moles of calcium pumped per mole of ATP hydrolyzed, as a measure of SERCA efficiency (98, 99). There are three micro-peptides known to modulate SERCA activity: phospholamban (PLN) (100), sarcolipin (SLN) (19, 20), and myoregulin (MLN) (101). PLN and MLN are very heart and skeletal muscle specific respectively and modulate SERCA by reducing its affinity for calcium (101). This causes a change in the rate of calcium pumping, but has no known consequence on coupling ratio. SLN on the other hand, increases the likelihood of "slippage," which results in the hydrolysis of an ATP without pumping any calcium (102). In vitro, it has been observed that as little as a 2:1 ratio of SLN:SERCA will cause a measurable reduction in coupling ratio (102). This loss of efficiency results in heat generation and contributes significantly to mammalian thermogenesis (20).

SERCA coupling ratio

Because the SERCA pump can account for up to 15% of whole-body resting metabolism and its efficiency can contribute significantly to thermogenesis, it is an ideal target for regulation in an animal with annual fluctuations in metabolic and thermoregulatory demands (16). To interrogate SERCA function, I developed a novel assay to measure its efficiency, or coupling ratio. We found that ATP hydrolysis is more coupled with calcium pumping in the spring than it is during hibernation (Figure 13). What this could mean is that their muscles are more able to produce heat during the hibernation season, similar to what is seen in cold-acclimation of non-hibernator muscles (103).

This shift in calcium handling efficiency likely has a role beyond SERCA-based thermogenesis though, since a reduction in calcium clearance by SERCA can have vast signaling effects (104). In both cold-acclimation and in the months prior to hibernation, there is a transition to a slower-twitch muscle phenotype (Figure 9) (105). Much of this transition can likely be attributed to the activity of the transcriptional coactivator PGC-1α (47, 105), which shows increased expression immediately prior to hibernation (Figure 4). Mice overexpressing skeletal muscle PGC-1α have reduced expression of key calcium handling proteins such as RYR1 and SERCA, while having increased expression of SERCA inhibitors PLN and SLN (104). The consequences of this altered expression are two-fold: first, there is less SERCA present to pump calcium, potentially slowing calcium clearance from the cytosol; and second, the SERCA that is there is less efficient slowing calcium clearance even further (104). Our proteomic data shows a variety of calcium handling proteins are lowest during the hibernation season, including SERCA1 (Figure 14). Contrary to what we would expect in the fast-to-slow transition, transcripts of SLN are also lowest during hibernation (Figure 15), indicating that if hibernator muscles were

following a canonical fast-to-slow transition, the efficiency of SERCA in hibernation might be even lower than we determined. Overall, this altered expression of calcium handling proteins, and reduced efficiency of SERCA during hibernation likely indicates a reduction in calcium clearance leading to the fiber-type transition observed in hibernator skeletal muscle (Figure 9) (104). Determining protein levels of SLN will be an important first step in determining the mechanism contributing to the reduced SERCA efficiency we see during hibernation.

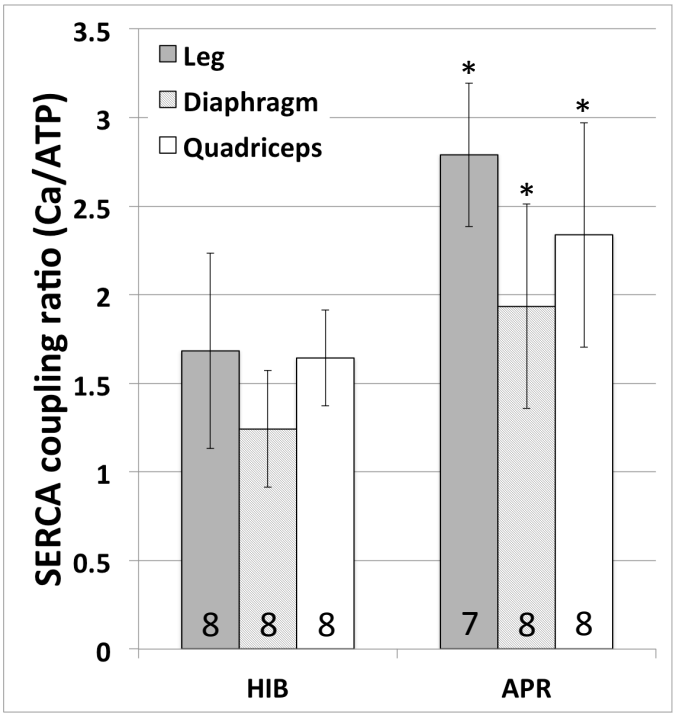

Figure 13. SERCA coupling ratio in hibernation and spring. Calcium uptake by SR vesicles was measured given limiting amounts of ATP using a calcium electrode system. Muscle groups represent fast (quadriceps), slow (diaphragm), and mixed (leg) muscle fiber types. All muscle groups show a significant increase in SERCA coupling ratio in APR relative to HIB ($p<0.05$).

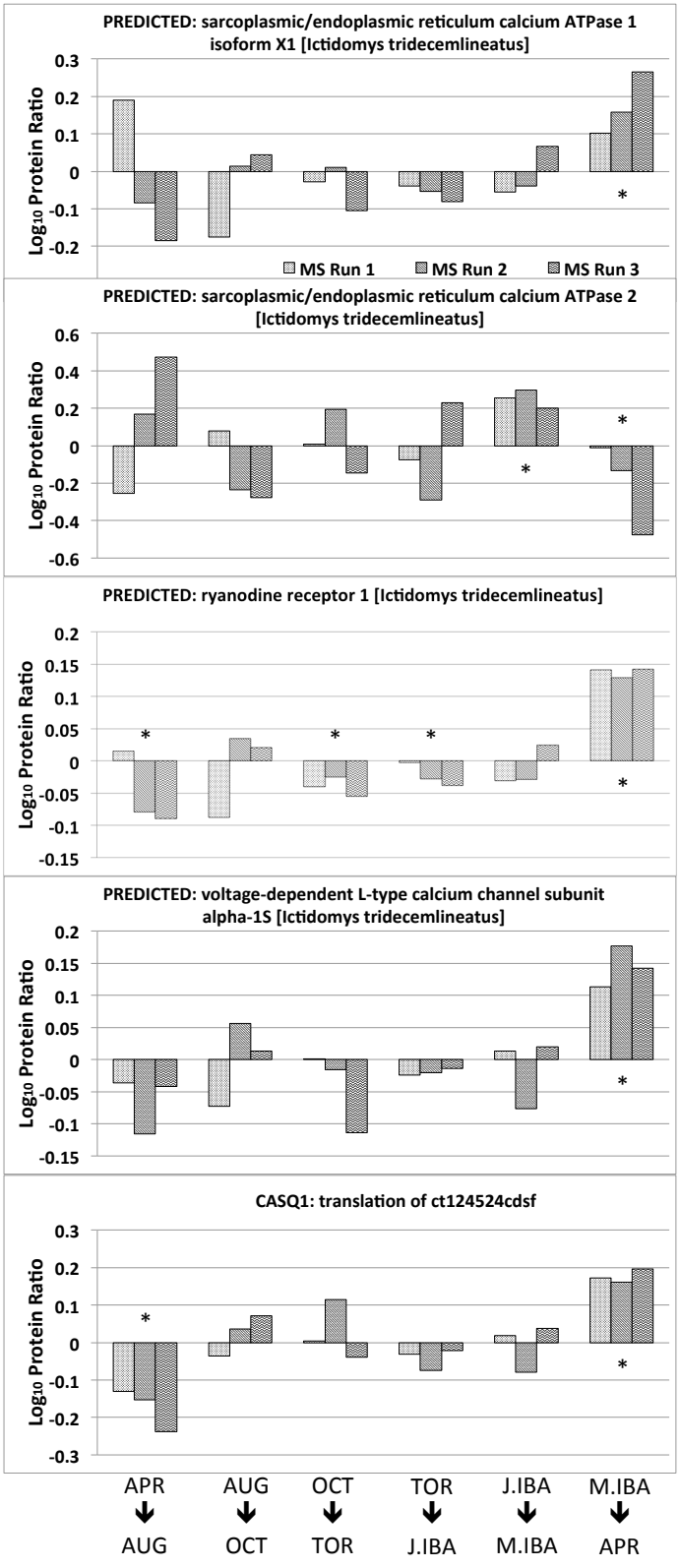

Figure 14. Expression profiles of calcium handling proteins in hibernator skeletal muscle. Protein identification and quantification were obtained by iTRAQ labeling and MS/MS proteomics. The three MS runs are represented independently with an asterisk indicating a significant difference (up or down) at the specified comparison point. Many of these calcium handling proteins are at their lowest during hibernation and increase upon spring arousal.

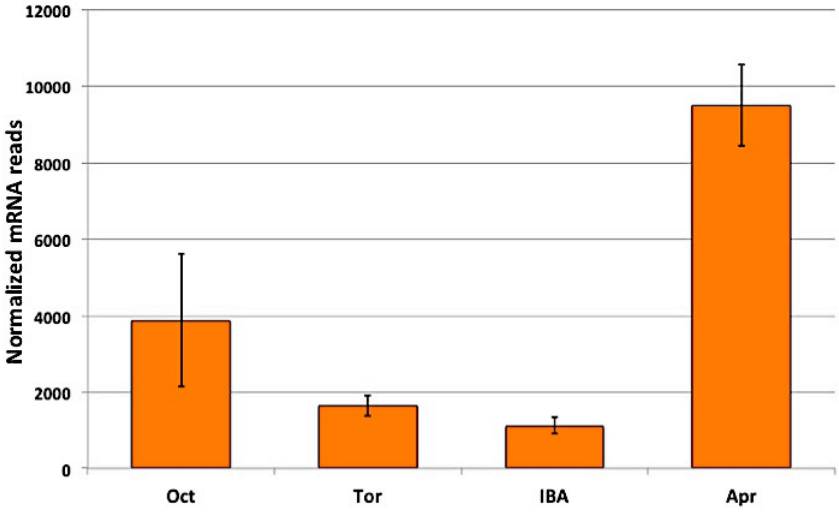

Figure 15. Sarcolipin gene expression. Illumina HiSeq2000 sequencing technology was used to determine gene expression at four time points throughout the circannual cycle. This gene was not identified by the initial screen because of its small size. There is nearly a 10-fold increase in expression from hibernation to spring.

Future Directions

As of 4/24/2016, all SR samples used in the above analysis have been collected. Thus far we have only been able to complete the SERCA efficiency assay. The next step will be to confirm protein levels for SLN and SERCA from these samples. I have worked out methods that work well to Western blot for each of these proteins from the very hydrophobic samples. Based on the SERCA efficiency results (Figure 13) I would suspect SERCA to drop significantly during hibernation and SLN to remain constant. I plan to start these in the next few weeks and to train an undergraduate (Anton Sauer) and a future graduate student (Rebecca Madden) on these protocols.

I have also been training these two on how to do the SR isolations and the SERCA assay in order to optimize and further validate the assay. While I have informally done some validation of this assay, I don't have enough for statistical support. The first most important assumption is that this assay, by providing a ratio, should be independent of the total protein added to the reaction chamber. This assumes that all of

the ATP added is used by the SRs present in the chamber, regardless of their abundance. They will test this assumption by using rat muscle to isolate SR vesicles and run the SERCA assay with varying amounts of protein. I have informally done this a few times and do not expect any significant change in coupling ratio until SR concentrations are so low that the vesicles can no longer physically load any more calcium.

Another important aspect of this assay is that the ratio measured is always much higher than would be expected from the literature. The theoretical optimal coupling ratio of SERCA is 2 calcium ions pumped per ATP hydrolyzed (106), but this assay clearly measures higher values (Figure 13). This is likely due to the presence of adenylate kinase in the SR preps. This enzyme is highly abundant in skeletal muscle and catalyzes the initerconversion of adenine nucleotides, thus recycling the ADP produced by SERCA back into ATP and AMP. This conversion should go to completion in all samples, regardless of muscle type or time of year, and thus should have no effect on the observed difference. By fueling identical samples with both ATP and ADP, we would be able to determine the true coupling ratio and could compare to literature values more accurately.

The final assumption is that the SLN:SERCA ratio is the primary cause for the change in SERCA efficiency. Because SLN is a small protein, only 33 amino acids long, we have had synthesized a peptide matching the squirrel sequence. With the addition of this peptide to SR vesicles we should be able to reduce SERCA efficiency in an equivalent manner to what is seen between SPR and HIB (Figure 13). This experiment would be performed after thorough western blotting of the current samples to ensure that we could artificially match the SLN:SERCA ratio present in HIB and APR, and determine if the change in coupling ratio is similar.

References

1. Lyman C.P. Who is among the hibernators. *Hibernation and Torpor in mammals and birds,* edited by Lyman C.P, Willis J.S., Malan A., and Wnag L.C.H. New York: Academic Press, **1982**, 12-36.
2. Andrews MT. Advances in molecular biology of hibernation in mammals. *Bioessays* **2007**, *29,* 431-440.
3. Carey HV, Andrews MT, and Martin SL. Mammalian hibernation: cellular and molecular responses to depressed metabolism and low temperature. *Physiol Rev.* **2003**, 83: 1153-1181.
4. Smith, RE. Thermogenic activity of the hibernating gland in the cold-acclimated rat. *Physiologist* **1961**, 113.
5. Cannon, B. Brown Adipose Tissue: Function and Physiological Significance. *Physiol. Rev.* **2004**, *84* (1), 277–359.
6. Schwartz, C.; Hampton, M.; Andrews, M. T. Hypothalamic Gene Expression Underlying Pre-Hibernation Satiety. *Genes, Brain Behav.* **2015**, *14* (3), 310–318.
7. Wang, LCH. Energetics and field aspects of mammalian torpor: The Richerdson's ground squirrel. *Strategies in Cold: Natural Torpidity and Thermogenesis.* Edited by Wang LCH and Hudson JW. New York: Academic Press, **1978**, p. 109-145
8. Van Breukelen, F.; Martin, S. L. Reversible Depression of Transcription during Hibernation. *J. Comp. Physiol. B Biochem. Syst. Environ. Physiol.* **2002**, *172* (5), 355–361.
9. Van Breukelen, F.; Martin, S. L. Translational Initiation Is Uncoupled from Elongation at 18 Degrees C during Mammalian Hibernation. *Am. J. Physiol. Regul. Integr. Comp. Physiol.* **2001**, *281* (5), R1374–R1379.
10. Zurlo, F.; Larson, K.; Bogardus, C.; Ravussin, E. Skeletal Muscle Metabolism Is a Major Determinant of Resting Energy Expenditure. *J. Clin. Invest.* **1990**, *86* (5), 1423–1427.
11. Schiaffino, S.; Reggiani, C. Fiber Types in Mammalian Skeletal Muscles. *Physiol.*
12. Barnard, RJ. Edgerton, VR. Furukava, T. Peter, JB. Histochemical, biochemical, and contractile properties of red, white, and intermediate fibers. *Am J Physiol* **1971**, 220, 410-414
13. Pette, D.; Staron, R. S. Myosin Isoforms, Muscle Fiber Types, and transitions1. *Microsc.Res.Tech.* **2000**, *50* (6), 500–509.
14. Glass, D. J. Skeletal Muscle Hypertrophy and Atrophy Signaling Pathways. *Int. J. Biochem. Cell Biol.* **2005**, *37* (10), 1974–1984.
15. Stevenson, E. J.; Giresi, P. G.; Koncarevic, A.; Kandarian, S. C. Global Analysis of Gene Expression Patterns during Disuse Atrophy in Rat Skeletal Muscle. *J. Physiol.* **2003**, *551* (1), 33–48.
16. Smith, I. C.; Bombardier, E.; Vigna, C.; Tupling, a. R. ATP Consumption by Sarcoplasmic Reticulum Ca2+ Pumps Accounts for 40-50% of Resting Metabolic Rate in Mouse Fast and Slow Twitch Skeletal Muscle. *PLoS One* **2013**, *8* (7), 1–11.
17. Toyoshima, C. Structural aspects of ion pumping by Ca^{2+} -ATPase of sarcoplasmic reticulum. *Arch. Biochem. Biophys.* **2008**, 476, 3-11
18. Arruda, A. P.; Da-Silva, W. S.; Carvalho, D. P.; De Meis, L. Hyperthyroidism Increases the Uncoupled ATPase Activity and Heat Production by the Sarcoplasmic Reticulum Ca2+-ATPase. *Biochem. J.* **2003**, *375*, 753–760.
19. Sahoo, S. K.; Shaikh, S. A.; Sopariwala, D. H.; Bal, N. C.; Periasamy, M. Sarcolipin Protein Interaction with Sarco(endo)plasmic Reticulum Ca2+ATPase (SERCA) Is Distinct from Phospholamban Protein, and Only Sarcolipin Can Promote Uncoupling of the SERCA Pump. *J. Biol. Chem.* **2013**, *288* (10), 6881–6889.
20. Bal, N. C.; Maurya, S. K.; Sopariwala, D. H.; Sahoo, S. K.; Gupta, S. C.; Shaikh, S. a; Pant, M.; Rowland, L. a; Goonasekera, S. a; Molkentin, J. D.; Periasamy, M. Sarcolipin Is a Newly Identified Regulator of Muscle-Based Thermogenesis in Mammals. *Nat. Med.* **2012**, *18* (10), 1575–1579.

21. Andres-Mateos, E.; Brinkmeier, H.; Burks, T. N.; Mejias, R.; Files, D. C.; Steinberger, M.; Soleimani, A.; Marx, R.; Simmers, J. L.; Lin, B.; Finanger Hedderick, E.; Marr, T. G.; Lin, B. M.; Hourdé, C.; Leinwand, L. A.; Kuhl, D.; Föller, M.; Vogelsang, S.; Hernandez-Diaz, I.; Vaughan, D. K.; Alvarez de la Rosa, D.; Lang, F.; Cohn, R. D. Activation of Serum/glucocorticoid-Induced Kinase 1 (SGK1) Is Important to Maintain Skeletal Muscle Homeostasis and Prevent Atrophy. *EMBO Mol. Med.* **2013**, *5* (1), 80–91.
22. Nowell, M. M.; Choi, H.; Rourke, B. C. Muscle Plasticity in Hibernating Ground Squirrels (Spermophilus Lateralis) Is Induced by Seasonal, but Not Low-Temperature, Mechanisms. *J. Comp. Physiol. B.* **2011**, *181* (1), 147–164.
23. Xu, R.; Andres-Mateos, E.; Mejias, R.; MacDonald, E. M.; Leinwand, L. A.; Merriman, D. K.; Fink, R. H. A.; Cohn, R. D. Hibernating Squirrel Muscle Activates the Endurance Exercise Pathway despite Prolonged Immobilization. *Exp. Neurol.* **2013**, *247*, 392–401.
24. Lee, K.; Joo, Y. P.; Yoo, W.; Gwag, T.; Lee, J. W.; Byun, M. W.; Choi, I. Overcoming Muscle Atrophy in a Hibernating Mammal despite Prolonged Disuse in Dormancy: Proteomic and Molecular Assessment. *J. Cell. Biochem.* **2008**, *104* (2), 642–656.
25. Brooks, N. E.; Myburgh, K. H.; Storey, K. B. Myostatin Levels in Skeletal Muscle of Hibernating Ground Squirrels. *J. Exp. Biol.* **2011**, *214*, 2522–2527.
26. Hindle, A. G.; Otis, J. P.; Epperson, L. E.; Hornberger, T. A.; Goodman, C. A.; Carey, H. V.; Martin, S. L. Prioritization of Skeletal Muscle Growth for Emergence from Hibernation. *J. Exp. Biol.* **2014**, *218* (2), 276–284.
27. Vermillion, K. L.; Anderson, K. J.; Hampton, M.; Andrews, M. T. Gene Expression Changes Controlling Distinct Adaptations in the Heart and Skeletal Muscle of a Hibernating Mammal. *Physiol. Genomics* **2015**, *47* (3), physiolgenomics.00108.2014.
28. Brauch, K. M.; Dhruv, N. D.; Hanse, E. a; Andrews, M. T.; Katharine, M.; Dhruv, N. D.; Hanse, E. a; Andrews, M. T. In the Heart of a Hibernating Mammal. **2005**, *29*, 227–234.
29. Anderson, K. J.; Vermillion, K. L.; Jagtap, P.; Johnson, J. E.; Griffin, T. J.; Andrews, M. T. Proteogenomic Analysis of a Hibernating Mammal Indicates Contribution of Skeletal Muscle Physiology to the Hibernation Phenotype. *J. Proteome Res.* **2016**, *15* (4), 1253-1261.
30. Grabherr MG, Haas BJ, Yassour M, Levin JZ, Thompson DA, Amit I, Adiconis X, Fan L, Raychowdhury R, Zeng Q, Chen Z, Mauceli E, Hacohen N, Gnirke A, Rhind N, di Palma F, Birren BW, Nusbaum C, Lindblad-Toh K, Friedman N, and Regev A. Full-length transcriptome assembly from RNA-Seq data without a reference genome. *Nat Biotechnol* **2011**, *29*, 644-652.
31. Schwartz C, Hampton M, and Andrews MT. Seasonal and regional differences in gene expression in the brain of a hibernating mammal. *PLoS One* 8: e58427, 2013.
32. Hampton M, Melvin RG, Kendall AH, Kirkpatrick BR, Peterson N, and Andrews MT. Deep sequencing the transcriptome reveals seasonal adaptive mechanisms in a hibernating mammal. *PLoS One* **2011**, *6*, e27021.
33. Altschul SF, Madden TL, Schaffer AA, Zhang J, Zhang Z, Miller W, and Lipman DJ. Gapped BLAST and PSI-BLAST: a new generation of protein database search programs. *Nucleic Acids Res* **1997**, *25*, 3389-3402.
34. Anders S, and Huber W. Differential expression analysis for sequence count data. *Genome Biol* **2010**, *11*, R106.
35. Hampton, M.; Melvin, R. G.; Andrews, M. T. Transcriptomic Analysis of Brown Adipose Tissue across the Physiological Extremes of Natural Hibernation. *PLoS One* **2013**, *8* (12), e85157.
36. Bourgon R, Gentleman R, and Huber W. Independent filtering increases detection power for high-throughput experiments. *Proc Natl Acad Sci U S A* **2010**, 107: 9546-9551.
37. Huang da W, Sherman BT, Stephens R, Baseler MW, Lane HC, and Lempicki RA. DAVID gene ID conversion tool. *Bioinformation* **2008**, *2*, 428-430.
38. Huang da W, Sherman BT, Tan Q, Collins JR, Alvord WG, Roayaei J, Stephens R, Baseler MW, Lane HC, and Lempicki RA. The DAVID Gene Functional Classification Tool: a

novel biological module-centric algorithm to functionally analyze large gene lists. *Genome Biol* **2007**, *8*, R183.
39. Breton S. The cellular physiology of carbonic anhydrases. *JOP : Journal of the pancreas* **2001**, *2*,159-164.
40. Endo, S.; Matsunaga, T.; Kuragano, T.; Ohno, S.; Kitade, Y.; Tajima, K.; El-Kabbani, O.; Hara, A. Properties and Tissue Distribution of a Novel Aldo-Keto Reductase Encoding in a Rat Gene (Akr1b10). *Arch. Biochem. Biophys.* **2010**, *503* (2), 230–237.
41. Itsui, Y.; Sakamoto, N.; Kakinuma, S.; Nakagawa, M.; Sekine-Osajima, Y.; Tasaka-Fujita, M.; Nishimura-Sakurai, Y.; Suda, G.; Karakama, Y.; Mishima, K.; Yamamoto, M.; Watanabe, T.; Ueyama, M.; Funaoka, Y.; Azuma, S.; Watanabe, M. Antiviral Effects of the Interferon-Induced Protein Guanylate Binding Protein 1 and Its Interaction with the Hepatitis C Virus NS5B Protein. *Hepatology* **2009**, *50* (6), 1727–1737.
42. Carriere V, Barbat A, Rousset M, Brot-Laroche E, Dussaulx E, Cambier D, De Waziers ID, Beaune P, and Zweibaum A. Regulation of sucrase-isomaltase and hexose transporters in Caco-2 cells: a role for cytochrome P-4501A1? *Am J Physiol.* **1996**, *270*, 976-986.
43. Carriere V, Rodolosse A, Lacasa M, Cambier D, Zweibaum A, and Rousset M. Hypoxia and CYP1A1 induction-dependent regulation of proteins involved in glucose utilization in Caco-2 cells. *Am J Physiol.* **1998**, *274*, 1101-1108.
44. Grabek KR, Karimpour-Fard A, Epperson LE, Hindle A, Hunter LE, and Martin SL. Multistate proteomics analysis reveals novel strategies used by a hibernator to precondition the heart and conserve ATP for winter heterothermy. *Physiol Genomics* **2011**, *43*, 1263-1275.
45. Luque A, Carpizo DR, and Iruela-Arispe ML. ADAMTS1/METH1 inhibits endothelial cell proliferation by direct binding and sequestration of VEGF165. *J Biol Chem* **2003**, *278*, 23656-23665,.
46. Vazquez F, Hastings G, Ortega MA, Lane TF, Oikemus S, Lombardo M, and Iruela-Arispe ML. METH-1, a human ortholog of ADAMTS-1, and METH-2 are members of a new family of proteins with angio-inhibitory activity. *J Biol Chem* **1999**, *274*, 23349-23357,.
47. Finck, B. N.; Kelly, D. P. PGC-1 Coactivators: Inducible Regulators of Energy Metabolism in Health and Disease. *J. Clin. Invest.* **2006**, *116* (3), 615–622.
48. Andrews MT, Squire TL, Bowen CM, and Rollins MB. Low-temperature carbon utilization is regulated by novel gene activity in the heart of a hibernating mammal. *Proc Natl Acad Sci U S A* **1998**, *95*, 8392-8397,.
49. Yokota S, and Asayama K. Peroxisomes of the rat cardiac and soleus muscles increase after starvation. A biochemical and immunocytochemical study. *Histochemistry* **1990**, *93*, 287-293,.
50. Jagoe RT, Lecker SH, Gomes M, and Goldberg AL. Patterns of gene expression in atrophying skeletal muscles: response to food deprivation. *Faseb J* **2002**, *16*, 1697-1712.
51. Van der Lee KA, Willemsen PH, Samec S, Seydoux J, Dulloo AG, Pelsers MM, Glatz JF, Van der Vusse GJ, and Van Bilsen M. Fasting-induced changes in the expression of genes controlling substrate metabolism in the rat heart. *Journal of lipid research* **2001**, *42*, 1752-1758.
52. Holloway GP, Chou CJ, Lally J, Stellingwerff T, Maher AC, Gavrilova O, Haluzik M, Alkhateeb H, Reitman ML, and Bonen A. Increasing skeletal muscle fatty acid transport protein 1 (FATP1) targets fatty acids to oxidation and does not predispose mice to diet-induced insulin resistance. *Diabetologia* **2011**, *54*, 1457-1467.
53. DiRusso CC, Li H, Darwis D, Watkins PA, Berger J, and Black PN. Comparative biochemical studies of the murine fatty acid transport proteins (FATP) expressed in yeast. *J Biol Chem* **2005**, *280*, 16829-16837.
54. Hentze MW, Muckenthaler MU, and Andrews NC. Balancing acts: molecular control of mammalian iron metabolism. *Cell* **2004**, *117*, 285-297.
55. Postnikova GB, Tselikova SV, Kolaeva SG, and Solomonov NG. Myoglobin content in skeletal muscles of hibernating ground squirrels rises in autumn and winter.

Comparative biochemistry and physiology Part A, Molecular & integrative physiology **1999**, *124*, 35-37.
56. Noren SR, and Williams TM. Body size and skeletal muscle myoglobin of cetaceans: adaptations for maximizing dive duration. *Comparative biochemistry and physiology Part A, Molecular & integrative physiology* **2000**, *126*, 181-191.
57. Toien O, Drew KL, Chao ML, and Rice ME. Ascorbate dynamics and oxygen consumption during arousal from hibernation in Arctic ground squirrels. *Am J Physiol Regul Integr Comp Physiol* **2001**, *281*, R572-583.
58. Arany Z, Foo SY, Ma Y, Ruas JL, Bommi-Reddy A, Girnun G, Cooper M, Laznik D, Chinsomboon J, Rangwala SM, Baek KH, Rosenzweig A, and Spiegelman BM. HIF-independent regulation of VEGF and angiogenesis by the transcriptional coactivator PGC-1alpha. *Nature* **2008**, *451*, 1008-1012.
59. Lin J, Handschin C, and Spiegelman BM. Metabolic control through the PGC-1 family of transcription coactivators. *Cell metabolism* **2005**, *1*, 361-370.
60. Booth FW. Effect of limb immobilization on skeletal muscle. *Journal of applied physiology: respiratory, environmental and exercise physiology* **1982**, *52*, 1113-1118.
61. Li JB, and Goldberg AL. Effects of food deprivation on protein synthesis and degradation in rat skeletal muscles. *Am J Physiol* **1976,** *231*, 441-448.
62. Phillips SM, Glover EI, and Rennie MJ. Alterations of protein turnover underlying disuse atrophy in human skeletal muscle. *Journal of applied physiology* **2009**, *107*, 645-654.
63. Ochi E, Ishii N, and Nakazato K. Time Course Change of IGF1/Akt/mTOR/p70s6k Pathway Activation in Rat Gastrocnemius Muscle During Repeated Bouts of Eccentric Exercise. *Journal of sports science & medicine* **2010**, *9*, 170-175.
64. Lee K, So H, Gwag T, Ju H, Lee JW, Yamashita M, and Choi I. Molecular mechanism underlying muscle mass retention in hibernating bats: role of periodic arousal. *Journal of cellular physiology* **,** *222*, 313-319.
65. Sandri M, Lin J, Handschin C, Yang W, Arany ZP, Lecker SH, Goldberg AL, and Spiegelman BM. PGC-1alpha protects skeletal muscle from atrophy by suppressing FoxO3 action and atrophy-specific gene transcription. *Proc Natl Acad Sci U S A* **2006**, *103*, 16260-16265.
66. Stitt TN, Drujan D, Clarke BA, Panaro F, Timofeyva Y, Kline WO, Gonzalez M, Yancopoulos GD, and Glass DJ. The IGF-1/PI3K/Akt pathway prevents expression of muscle atrophy-induced ubiquitin ligases by inhibiting FOXO transcription factors. *Molecular cell* **2004,** 14, 395-403.
67. Schiaffino S, Dyar KA, Ciciliot S, Blaauw B, and Sandri M. Mechanisms regulating skeletal muscle growth and atrophy. *The FEBS journal* 280: 4294-4314, 2013.
68. Li H, Malhotra S, and Kumar A. Nuclear factor-kappa B signaling in skeletal muscle atrophy. *Journal of molecular medicine* **2008**, *86*, 1113-1126.
69. Kumar A, Bhatnagar S, and Paul PK. TWEAK and TRAF6 regulate skeletal muscle atrophy. *Current opinion in clinical nutrition and metabolic care* **2012,** *15*, 233-239.
70. Vermillion, K. L.; Jagtap, P.; Johnson, J. E.; Griffin, T. J.; Andrews, M. T. Characterizing Cardiac Molecular Mechanisms of Mammalian Hibernation via Quantitative Proteogenomics. *J. Proteome Res.* **2015**, *14* (11), 4792-4804.
71. Yang, F.; Shen, Y.; Camp, D. G.; Smith, R. D. High-pH Reversed-Phase Chromatography with Fraction Concatenation for 2D Proteomic Analysis. *Expert Rev. Proteomics* **2012**, *9* (2), 129–134.
72. Jagtap, P. D.; Johnson, J. E.; Onsongo, G.; Sadler, F. W.; Murray, K.; Wang, Y.; Shenykman, G. M.; Bandhakavi, S.; Smith, L. M.; Griffin, T. J. Flexible and Accessible Workflows for Improved Proteogenomic Analysis Using the Galaxy Framework. *J. Proteome Res.* **2014**, *13* (12), 5898–5908.
73. Russeth, K. P.; Higgins, L.; Andrews, M. T. Identification of Proteins from Non-Model Organisms Using Mass Spectrometry: Application to a Hibernating Mammal. *J. Proteome Res.* **2006**, *5* (4), 829–839.

74. Hindle, a. G.; Karimpour-Fard, a.; Epperson, L. E.; Hunter, L. E.; Martin, S. L. Skeletal Muscle Proteomics: Carbohydrate Metabolism Oscillates with Seasonal and Torpor-Arousal Physiology of Hibernation. *AJP Regul. Integr. Comp. Physiol.* **2011**, *301* (5), R1440–R1452.
75. Bielewicz, J.; Zanin, M. E.; Galbani, A.; Carraro, U. Contractile Proteins Content of Long Term Permanent Denervated Human Muscle after Functional Electrical Stimulation. *Basic Appl. Myol* **2004**, *14* (2), 83–86.
76. Russell, R. L.; O'Neill, P. H.; Epperson, L. E.; Martin, S. L. Extensive Use of Torpor in 13-Lined Ground Squirrels in the Fall prior to Cold Exposure. *J. Comp. Physiol. B* **2010**, *180* (8), 1165–1172.
77. Hardie, D. G.; Salt, I. P.; Hawley, S. A.; Davies, S. P. Cellular Energy Charge. *Biochem J.* **1999**, *338*, 717–722.
78. Hardie, D. G. Minireview: The AMP-Activated Protein Kinase Cascade: The Key Sensor of Cellular Energy Status. *Endocrinology* **2003**, *144* (12), 5179–5183.
79. Hardie, D. G.; Ross, F. a.; Hawley, S. a. AMPK: A Nutrient and Energy Sensor That Maintains Energy Homeostasis. *Nat. Rev. Mol. Cell Biol.* **2012**, *13* (4), 251–262.
80. Zong, H.; Ren, J. M.; Young, L. H.; Pypaert, M.; Mu, J.; Birnbaum, M. J.; Shulman, G. I. AMP Kinase Is Required for Mitochondrial Biogenesis in Skeletal Muscle in Response to Chronic Energy Deprivation. *Proc. Natl. Acad. Sci. U. S. A.* **2002**, *99* (25), 15983–15987.
81. Lee, W. J.; Kim, M.; Park, H.-S.; Kim, H. S.; Jeon, M. J.; Oh, K. S.; Koh, E. H.; Won, J. C.; Kim, M.-S.; Oh, G. T.; Yoon, M.; Lee, K.-U.; Park, J.-Y. AMPK Activation Increases Fatty Acid Oxidation in Skeletal Muscle by Activating PPARα and PGC-1. *Biochem. Biophys. Res. Commun.* **2006**, *340* (1), 291–295.
82. Jäger, S.; Handschin, C.; St-Pierre, J.; Spiegelman, B. M. AMP-Activated Protein Kinase (AMPK) Action in Skeletal Muscle via Direct Phosphorylation of PGC-1alpha. *Proc. Natl. Acad. Sci. U. S. A.* **2007**, *104* (29), 12017–12022.
83. Chapman, A. G.; Atkinson, D. E. Stabilization of Adenylate Energy Charge by the Adenylate Deaminase Reaction. *J. Biol. Chem.* **1973**, *248* (23), 8309–8312.
84. Plaideau, C.; Lai, Y.-C.; Kviklyte, S.; Zanou, N.; Löfgren, L.; Andersén, H.; Vertommen, D.; Gailly, P.; Hue, L.; Bohlooly-Y, M.; Hallén, S.; Rider, M. H. Effects of Pharmacological AMP Deaminase Inhibition and Ampd1 Deletion on Nucleotide Levels and AMPK Activation in Contracting Skeletal Muscle. *Chem. Biol.* **2014**, *21* (11), 1497–1510.
85. Norman, B.; Sabina, R. L.; Jansson, E. Regulation of Skeletal Muscle ATP Catabolism by AMPD1 Genotype during Sprint Exercise in Asymptomatic Subjects. *J. Appl. Physiol.* **2001**, *91* (1), 258–264.
86. Beal, P. R.; Yao, S. Y. M.; Baldwin, S. A.; Young, J. D.; King, A. E.; Cass, C. E. The Equilibrative Nucleoside Transporter Family, SLC29. *Pflugers Arch. Eur. J. Physiol.* **2004**, *447* (5), 735–743.
87. Zhang, J.; Kaasik, K.; Blackburn, M. R.; Lee, C. C. Constant Darkness Is a Circadian Metabolic Signal in Mammals. *Nature* **2006**, *439* (19), 340–343.
88. Swoap, S. J.; Rathvon, M.; Gutilla, M. AMP Does Not Induce Torpor. *Am. J. Physiol. Regul. Integr. Comp. Physiol.* **2007**, *293* (1), R468–R473.
89. Andres-Mateos, E.; Mejias, R.; Soleimani, A.; Lin, B. M.; Burks, T. N.; Marx, R.; Lin, B.; Zellars, R. C.; Zhang, Y.; Huso, D. L.; Marr, T. G.; Leinwand, L. a.; Merriman, D. K.; Cohn, R. D. Impaired Skeletal Muscle Regeneration in the Absence of Fibrosis during Hibernation in 13-Lined Ground Squirrels. *PLoS One* **2012**, *7* (11), 1–10.
90. Piersma, B.; Bank, R. A.; Boersema, M. Signaling in Fibrosis: TGF-β, WNT, and YAP/TAZ Converge. *Front. Med.* **2015**, *2* (September), 1–14.
91. Burks, T. N.; Cohn, R. D. Role of TGF-β Signaling in Inherited and Acquired Myopathies. *Skelet. Muscle* **2011**, *1* (1), 19.
92. Roberts, A. B.; McCune, B. K.; Sporn, M. B. TGF-β: Regulation of Extracellular Matrix. *Kidney Int.* **1992**, *41* (3), 557–559.

93. Zheng, Z.; Jian, J.; Zhang, X.; Zara, J. N.; Yin, W.; Chiang, M.; Liu, Y.; Wang, J.; Pang, S.; Ting, K.; Soo, C. Reprogramming of Human Fibroblasts into Multipotent Cells with a Single ECM Proteoglycan, Fibromodulin. *Biomaterials* **2012**, *33* (24), 5821–5831.
94. Hildebrand, A.; Romaris, M. Interaction of the Small Interstitial Proteoglycans Biglycan, Decorin and Fibromodulin with Transforming Growth Factor Beta. *Biochem. J.* **1994**, *534*, 527–534.
95. Soo, C.; Hu, F. Y.; Zhang, X.; Wang, Y.; Beanes, S. R.; Lorenz, H. P.; Hedrick, M. H.; Mackool, R. J.; Plaas, a; Kim, S. J.; Longaker, M. T.; Freymiller, E.; Ting, K. Differential Expression of Fibromodulin, a Transforming Growth Factor-Beta Modulator, in Fetal Skin Development and Scarless Repair. *Am. J. Pathol.* **2000**, *157* (2), 423–433.
96. Nesvizhskii, A. I. Proteogenomics: Concepts, Applications and Computational Strategies. *Nat. Methods* **2014**, *11* (11), 1114–1125.
97. Griffin, T. J. Complementary Profiling of Gene Expression at the Transcriptome and Proteome Levels in Saccharomyces Cerevisiae. *Mol. Cell. Proteomics* **2002**, *1* (4), 323–333.
98. Odermatt, A.; Kurzydlowski, K.; MacLennan, D. H. The V Max of the Ca 2+ - ATPase of Sarcoplasmic Reticulum (SERCA 2a) Is Not Altered by Ca 2+/ Calmodulin-Dependent Phosphorylation or by Interaction with Phospholamban. *J. Biol. Chem.* **1994**, *269* (24), 31198–31206.
99. McMullen, D. C.; Kean, W. S.; Verma, A.; Cole, J. T.; Watson, W. D. A Microplate Technique to Simultaneously Assay Calcium Accumulation in Endoplasmic Reticulum and SERCA Release of Inorganic Phosphate. *Biol. Proced. Online* **2012**, *14* (1), 4.
100. James, P., Inui, M., Tada, M., Chiesi, M. and Carafoli, E.,. Nature and site of phospholamban regulation of the Ca2+ pump of sarcoplasmic reticulum. *Nature*. **1989**, *342*(6245), 90-92.
101. Anderson, D. M.; Anderson, K. M.; Chang, C.; Makarewich, C. A.; Nelson, B. R.; Mcanally, J. R.; Kasaragod, P.; Shelton, J. M.; Liou, J.; Bassel-duby, R.; Olson, E. N. Regulates Muscle Performance. **2016**, *160* (4), 595–606.
102. Smith, W. S.; Broadbridge, R.; East, J. M.; Lee, A. G. Sarcolipin Uncouples Hydrolysis of ATP from Accumulation of Ca2+ by the Ca2+-ATPase of Skeletal-Muscle Sarcoplasmic Reticulum. *Biochem. J.* **2002**, *361* (Pt 2), 277–286.
103. Pant, M.; Bal, N. C.; Periasamy, M. Cold Adaptation Overrides Developmental Regulation of Sarcolipin Expression in Mice Skeletal Muscle: SOS for Muscle-Based Thermogenesis? *J. Exp. Biol.* **2015**, No. May, 2321–2325.
104. Summermatter, S.; Thurnheer, R.; Santos, G.; Mosca, B.; Baum, O.; Treves, S.; Hoppeler, H.; Zorzato, F.; Handschin, C. Remodeling of Calcium Handling in Skeletal Muscle through PGC-1 : Impact on Force, Fatigability, and Fiber Type. *AJP Cell Physiol.* **2012**, *302* (1), C88–C99.
105. Puigserver, P.; Wu, Z.; Park, C. W.; Graves, R.; Wright, M.; Spiegelman, B. M. A Cold-Inducible Coactivator of Nuclear Receptors Linked to Adaptive Thermogenesis. *Cell* **1998**, *92* (6), 829–839.
106. Tanford, C. Steady State of an ATP-Driven Calcium Pump: Limitations on Kinetic and Thermodynamic Parameters. *Proc. Natl. Acad. Sci. U. S. A.* **1982**, *79* (20), 6161–6165.